Paleoproterozoic potassic–ultrapotassic magmatism: Morro do Afonso Syenite Pluton, Bahia, Brazil

D.C. Rios [a,*], H. Conceição [a], D.W. Davis [b], J. Plá Cid [a], M.L.S. Rosa [a],
M.J.B. Macambira [c], I. McReath [d], M.M. Marinho [a,e], W.J. Davis [f]

[a] *Laboratory of Applied Petrology, Earth Sciences Institute, Federal University of Bahia, Rua Caetano Moura 123, 40.210-340 Salvador, BA, Brazil*
[b] *Jack Satterly Geochronological Laboratory, University of Toronto, Department of Geology, Earth Sciences Centre, 22 Russell Street, Toronto, Ont., Canada M5S 3B1*
[c] *Laboratory of Isotopic Geology, Federal University of Pará, Caixa Postal 1611, CEP 66075-900, Belém, PA, Brazil*
[d] *São Paulo University, Brazil*
[e] *Companhia Baiana de Pesquisa Mineral, 4ª Avenida 460, CAB, 41760-300 Salvador, BA, Brazil*
[f] *Geological Survey of Canada, 601 Booth St., Ottawa, Ont., Canada K1A 0E8*

Abstract

The Morro do Afonso Syenitic Pluton (MASP) is a small, bimodal suite of lamprophyric and syenitic rocks, located in the Serrinha Nucleus, São Francisco Craton, northeastern Brazil. The unit consists predominantly of alkali feldspar syenite with numerous mafic xenoliths and dykes that are predominantly lamprophyric.

The syenite shows geochemical and isotopic features typical of the Roman potassic magmas, i.e. low TiO_2 (up to 1.2%), low K_2O/Al_2O_3 (0.33–0.49), strong enrichment in LILE, and high LILE/HFSE ratios. Fractionation, mainly of clinopyroxene and amphibole, explains the transition from lamprophyre to syenite. Magma mixing is required to explain the most evolved compositions. MASP syenites have Paleoproterozoic crystallization ages (2.11 Ga). The Nd isotope composition of mafic and felsic phases are similar ($\varepsilon_{Nd_{mafic}} = -2.36$ to -2.61 and $\varepsilon_{Nd_{felsic}} = -2.47$) and they have Archaean model ages ($T_{DM} = 2.56$–2.58 Ga) that match the age of an inherited zircon grain (ca. 2.6 Ga).

MASP is similar to many other post-orogenic syenitic plutons distributed over a wide area of São Francisco Craton (SFC), which are closely comparable in age and also typically associated with ultrapotassic lamprophyre. The present results suggest that a major proportion of the potassic–ultrapotassic syenitic rocks of the SFC were emplaced in a narrow time interval from 2111 to 2080 Ma, limiting the time of metamorphism peak of the Transamazonian Orogeny to at least 2.1 Ga. These plutons show some evidence of having interactions with older felsic crustal rocks and are interpreted to be derived from partial melting of lithospheric mantle that was enriched by subduction.

1. Introduction

This paper concerns the Morro do Afonso Syenitic Pluton (MASP), a complex intrusion belonging to the Paleoproterozoic alkaline-potassic magmatism of Serrinha Nucleus (SerN), São Francisco Craton (SFC),

* Corresponding author. Tel.: +55 71 2303 8585; fax: +55 71 3203 8591.
  E-mail address: debora@cpgg.ufba.br (D.C. Rios).

Bahia, Brazil (Fig. 1A). The SerN potassic–ultrapotassic syenitic suite includes the three stocks shown in Fig. 1B (1 = Morro do Afonso; 2 = Agulhas-Bananas; 3 = Serra do Pintado). They are intermediate in age among the three categories of Paleoproterozoic alkaline plutonic rocks: shoshonite (oldest), syenite, and K-granite (youngest).

All the syenitic stocks of SerN are situated within the southwestern area of SerN, which also contains a number of gold and massive sulphide deposits. Nearby, at the Maria Preta Au-Mine, the gold deposits are spatially associated with alkali syenite and lamprophyre (Barrueto, 1997).

Syenite–lamprophyre–gold associations such as the one that occurs at SerN have been related in the literature to orogenic as well as anorogenic environments (McNeil and Kerrich, 1986; Wyman and Kerrich, 1988, 1989; Rock, 1987; Rock et al., 1991; Rock and Groves, 1988; Müller and Groves, 1993). Accordingly, geodynamic interpretations of Transamazonian potassic magmatism fall into two principal categories, which either claim a key role for subduction processes in the mantle enrichment responsible for the very peculiar geochemical and isotopic signatures of these magmas (e.g. Beccaluva et al., 1991; Serri et al., 1993) or consider them as an expression of continental rift magmatism (Lavecchia and Stoppa, 1996).

In SFC terrains, syenite are commonly associated with lamprophyres and related to silica-saturated potassic suites (Conceição et al., 1995, 2002; Rios, 1998; Paim et al., 2002; Plá Cid et al., 2006), to carbonatitic complexes (Angico dos Dias, Silva et al., 1988) or to Neoproterozoic sodic suites (Souto, 1972; Rosa et al., 2006). Within a collisional context, SFC alkaline magmas are considered to represent a late to post-orogenic event (see references above).

The principal aim of this paper is to present and discuss new petrographic, geochemical (major and trace elements) and isotopic data (Rb–Sr, Sm–Nd isotopes and Pb–Pb and U–Pb zircon ages) on the main MASP rock types in order to understand the magmatic processes that produced them. In particular, the ultrapotassic nature and mechanisms of chemical variation will be discussed. The tectonic setting of emplacement and a comparison with other alkaline rocks located in Bahia State will be touched on briefly.

2. Geological outline

The Archaean–Paleoproterozoic terrains of SFC (Fig. 1A), have been grouped by Mascarenhas et al. (1979) into three ancient nuclei, interpreted as Archaean cratons (Serrinha in the northeast; Remanso, central; Guanambi, in the west) bounded by Paleoproterozoic orogenic belts. Although recent proposals to rename these Archaean rocks as "blocks" (e.g. Serrinha Block, Barbosa and Sabaté, 2004), we will keep Mascarenhas et al. (1979) model. These nuclei are composed of gneissic and migmatitic rocks, granites and volcano-sedimentary sequences. Igneous protoliths predominate in the Paleoproterozoic orogenic belts (Barbosa and Sabaté, 2004).

SerN forms a mega-ellipsoidal Archaean structure (>21.000 km^2) which remained rigid during the Transamazonian collisional event with the Salvador-Curaçá Mobile Belt (SCMB), to the west (Fig. 1A). In the east, SerN terrains are covered by Neoproterozoic as well as Phanerozoic sediments (Fig. 1B). Recent studies (see Rios et al., 1998, 2003, 2004) have revealed an increasingly detailed picture of SerN. The most relevant geologic and lithostratigraphic characteristics are summarized below.

The lithostratigraphic succession at SerN (Fig. 1B) consists dominantly of (i) an Archaean basement of gneissic–migmatitic and calc-alkaline to tonalite–trondhjemite–granodiorite (TTG) plutons, predominantly with rocks of granodioritic composition and N–S foliations; (ii) volcano-sedimentary sequences: the Paleoproterozoic Itapicuru River Greenstone Belt (IRGB), the most important gold producer of Bahia (Silva et al., 2001, Davison et al., 1988), and the Archaean–Paleoproterozoic Capim Group (Oliveira et al., 1998, 1999); (iii) Paleoproterozoic intrusions. Archaean crustal evolution was undoubtedly of great complexity based on ages of granitic plutons in the range 3.6–2.6 Ga and the presence of zircon xenocrysts with ages as old as 3.6 Ga (Rios et al., 2002). Currently there is no evidence for geological events over the period 2.6–2.2 Ga.

The Paleoproterozoic evolution of SerN is marked by distinct magmatic events associated with crustal shortening, folding and metamorphism, which occurred as part of the Transamazonian Orogeny. Paleoproterozoic granites constitute ca. 30% of the SerN area and show a wide range of petrographic and geochemical compositions that may reflect an evolution of the magma genesis with various contributions from mantle, mafic or sialic crust material (Rios, 2002). The Paleoproterozoic was an extensive period of magmatism at SerN, which occurred in several episodes over the time range 2.25–2.07 Ga (Rios et al., 2003). The earliest Paleoproterozoic granitic units (2.13–2.16 Ga), have normal calc-alkaline to subordinate TTG trends and metaluminous to peraluminous character. Alkaline magmatism is most prominently developed in the southwestern area
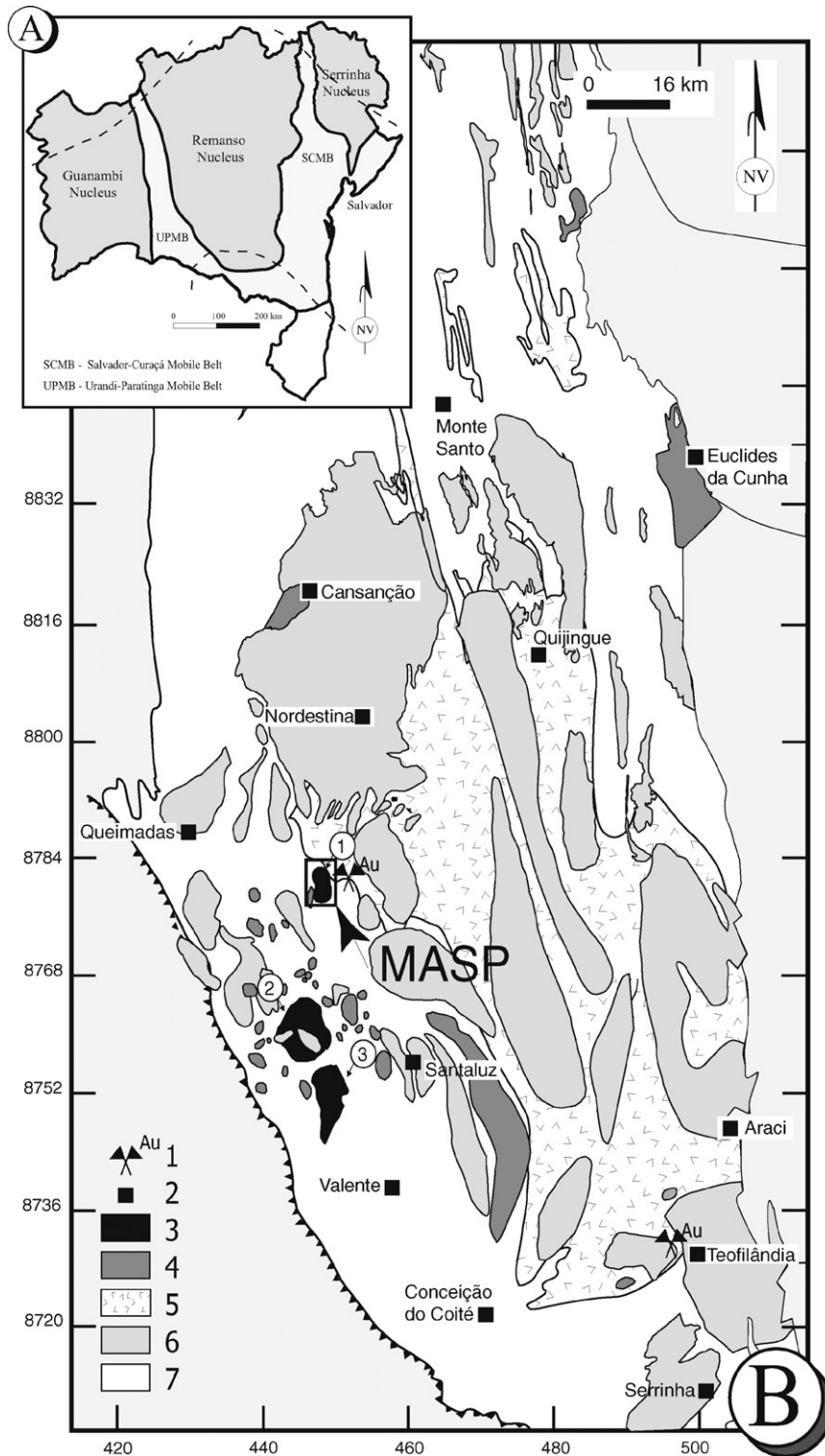
Fig. 1. (A) Geotectonic sketch map showing the major Paleoproterozoic Provinces of the São Francisco Craton, Bahia State, as proposed by Mascarenhas et al. (1979). (B) Simplified geological map of the Serrinha Nucleus (modified from Rios, 2002), showing the location of the studied syenite. Legend: (1) Au mines; (2) city; Paleoproterozoic: (3) syenites, (4) shoshonites, (5) volcano-sedimentary sequences; (6) Archaean and Paleoproterozoic calc-alkaline granites and TTGs; (7) gneissic–migmatitic basement.

of SerN and, as in many granite greenstone terrains worldwide (e.g. Abitibi greenstone belt, Canada, Wyman and Kerrich, 1993), makes up a distinct but volumetrically minor assemblage of rock types that post-dates the major volcanic–plutonic cycles and much of the early deformation. It varies from ultrapotassic (lamprophyres) to potassic (granodiorite, monzonite, syenite, syenodiorite) and shoshonitic (Fig. 1B). The latest units include peraluminous K-granites (~2.07 Ga; Rios et al., 2000).

Syenites occur as discrete intrusions, cutting the greenstone belts and/or the Archaean TTG suites. Syenite and shoshonite share some geochemical similarities and, as advocated for other similar terrains (e.g. Laflèche et al., 1991; Wyman and Kerrich, 1989), may have resulted from a primitive type of plate tectonics. Long-standing debates over the geodynamic setting of SerN largely concern subduction polarity, its age (Paleoproterozoic or Archaean), and even the existence of subduction (Jardim de Sá, 1982; Figueiredo, 1989; Silva, 1992; Alves da Silva et al., 1993; Alves da Silva, 1994; Cordani et al., 1985, 2000).

3. Sampling and analytical procedures

A total of 82 samples of MASP were collected from surface outcrops. The sampling program concentrated on the syenitic portion of the complex. Analyses of lamprophyre are given by Plá Cid et al. (2006).

3.1. Major and trace elements determination

Whole rock major and trace elements have been determined for 12 relatively fresh samples from the felsic syenite, 7 from the mafic syenite, and 2 from orthocumulate. The sample locations are displayed in Fig. 2.

Major and trace elements were analyzed at the Lakefied-GEOSOL Consortium Laboratories, by X-ray fluorescence spectrometry [Si, Al, Fe, Mg (0.10%), Ca, Ti, P, Mn, Cl, S, Ba, Cs, Ga, Hf (8 ppm), Nb, Rb, Sn, Sr, Ta, Th, U (10 ppm), V (8 ppm), Y, Zr, W (10 ppm), Sc (10 ppm)] with lithium tetraborate fusion or by atomic absorption (Na, K, Co, Cr, Cu, Ni and Pb) after multi-acid digestion (HF, HCl and perchloric acid). REE elements were determined by ICP-AES spectrometry. Detection limits were 1 ppm for REE, 0.01% for major elements and 5 ppm for trace elements, except where a different value is indicated under parentheses. For more details see Rios (1997, 2002).

3.2. Pb–Pb evaporation and U–Pb zircon geochronology

The samples were crushed and the zircon crystals were concentrated from each of the selected rock samples following standard mineral separation techniques (heavy liquids and magnetic separator). The zircon grains were hand picked from the least specific magnetic susceptibility fraction. The sorted crystals were examined under a binocular microscope and single grains were selected for analysis based on grouping into populations according to color, transparency, magmatic habit, and absence of cracks and inclusions.

Dating by the Pb–Pb evaporation technique (Köber, 1986) was performed at the Isotopic Laboratory of the Federal University of Pará (PARA-ISO, Brazil) using a Finnigan MAT-262 or VG Isomass 54E spectrometer. Decay constants are from Jaffey et al. (1971). Common lead is corrected using the two-stage terrestrial lead model of Stacey and Kramers (1975). Analyses with $^{206}Pb/^{204}Pb$ ratios of less than 2000 were not used because these may correspond to evaporation from altered domains which could give younger, discordant ages. The details of the technique used for the samples in this study are described in Gaudette et al. (1998).

U–Pb analyses were performed at the J.C. Roddick Ion Microprobe Laboratory, of the Geological Survey of Canada (GSC), Ottawa, Canada, using a Sensitive Resolution Ion Microprobe generation II (SHRIMP II), a Nier-Johnson type. The analytical methods of zircon U–Pb–Th age determinations using the SHRIMP of GSC are reported in details in Stern (1997). Analyses were performed using a 3 nA primary ion beam and a $10 \mu m \times 13 \mu m$ spot (70 μm Kohler aperture). Pb/U ratios were determined relative to standard BR266 (559 Ma and 910 ppm U). Standards were analyzed after every four unknowns to monitor the stability of calibration.

3.3. Isotope analyses

Rb, Sr, Sm and Nd were separated by standard cation exchange techniques from HCl-leached whole rock samples, and subsequently analyzed on a mass spectrometer at the University of São Paulo (USP, Brazil), according to procedures summarized in Sato et al. (1995). Elemental concentrations of Rb, Sr, Sm and Nd were determined by ICP-MS after dissolution by fusion at Activation Laboratories (Ancaster, Canada). Detection limits are 0.01 ppm for Sm and 0.05 ppm for Nd. Sr and Nd isotopic ratios are normalized to $^{86}Sr/^{88}Sr = 0.1194$

and $^{144}Nd/^{146}Nd = 0.7219$, respectively. The notations of ε_{Nd} and $f_{Sm/Nd}$ are defined according to common equations (Faure, 1986).

4. The Morro do Afonso potassic–ultrapotassic intrusion

MASP is an oval-shaped stock, $4\,km \times 3\,km$ (Fig. 2A), trending roughly N–S, which intrudes the metavolcanic rocks of IRGB and gneiss and migmatite of the Santa Luz Complex (Fig. 2A), showing a wide range of rock textures. The rocks consist essentially of mafic and felsic porphyritic syenite crosscut by lamprophyre dikes and containing numerous enclaves composed of: (i) autoliths and mafic cumulates containing mica, clinopyroxene, amphibole and apatite; (ii) mafic microgranular enclaves of lamprophyric composition; (iii) xenoliths from basement host rocks. MASP is discordant with respect to the surrounding Archaean basement of SerN, as well as the IRGB rocks, where it has formed a thin border of hornfels (Rios, 1998).

Rock types range from ultramafic (clinopyroxene–mica enclaves) to granite. Morro do Afonso intrusion is composed of three syenite members (Figs. 2 and 3A): (i) clinopyroxene-rich (ca. 20–30%) mafic syenite (Fig. 3B), (ii) alkali feldspar-rich (ca. 50%) felsic syenite (Fig. 3C), although its groundmass ranges from leuco to melanocratic according to the Streckeisen (1976) criteria, and (iii) orthoclase-cumulate (Fig. 3D). The mafic and felsic syenite components of MASP are distinguished by their relative proportions of alkali feldspar and clinopyroxene: mafic syenite, >20% modal clinopyroxene; felsic syenite, up to 11% modal diopside
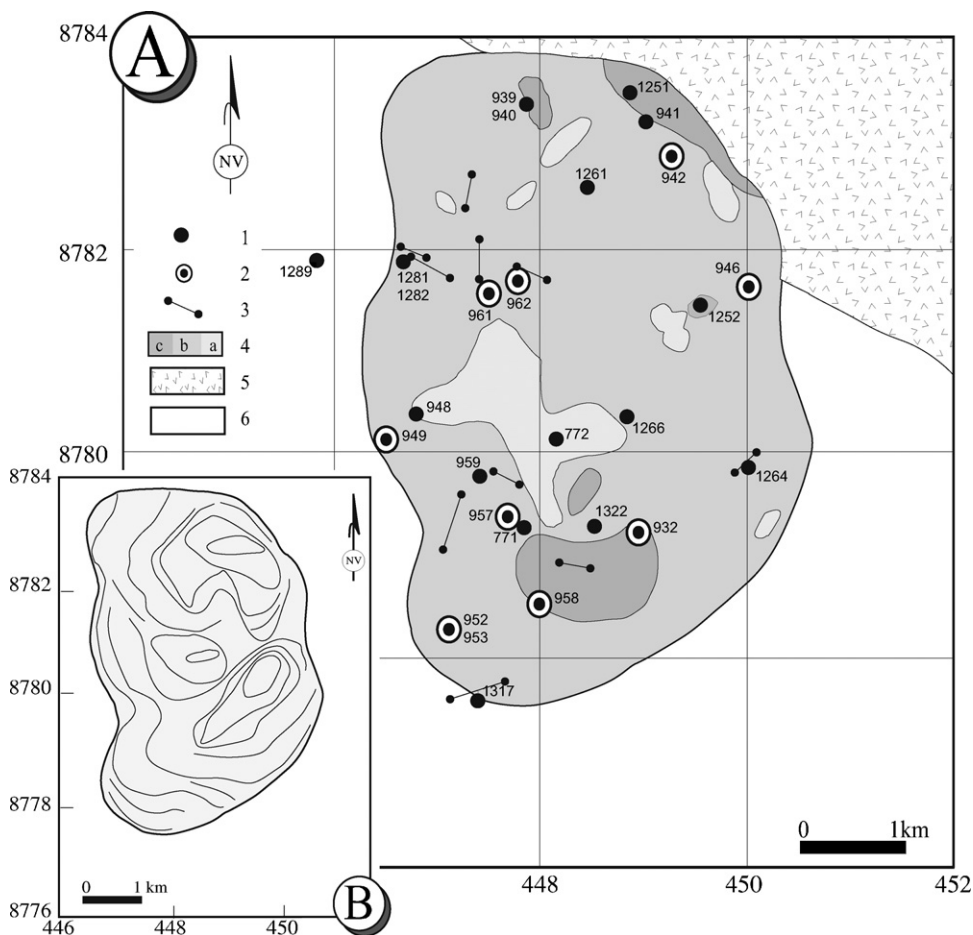
Fig. 2. (A) Geological map of Morro do Afonso Syenite Pluton, showing the location of studied samples. (1) Studied samples; (2) samples with geochronological and/or isotopic data; (3) lamprophyre dykes; (4) Morro do Afonso: (a) felsic syenite, (b) mafic syenite, (c) orthocumulate; (5) Itapicuru River Greenstone Belt: basal mafic volcanic unit; (6) basement rocks: banded gneisses and orthogneisses. (B) Schematic map of Morro do Afonso Syenite Pluton showing the magmatic flow foliation trends (modified from Rios, 1998).
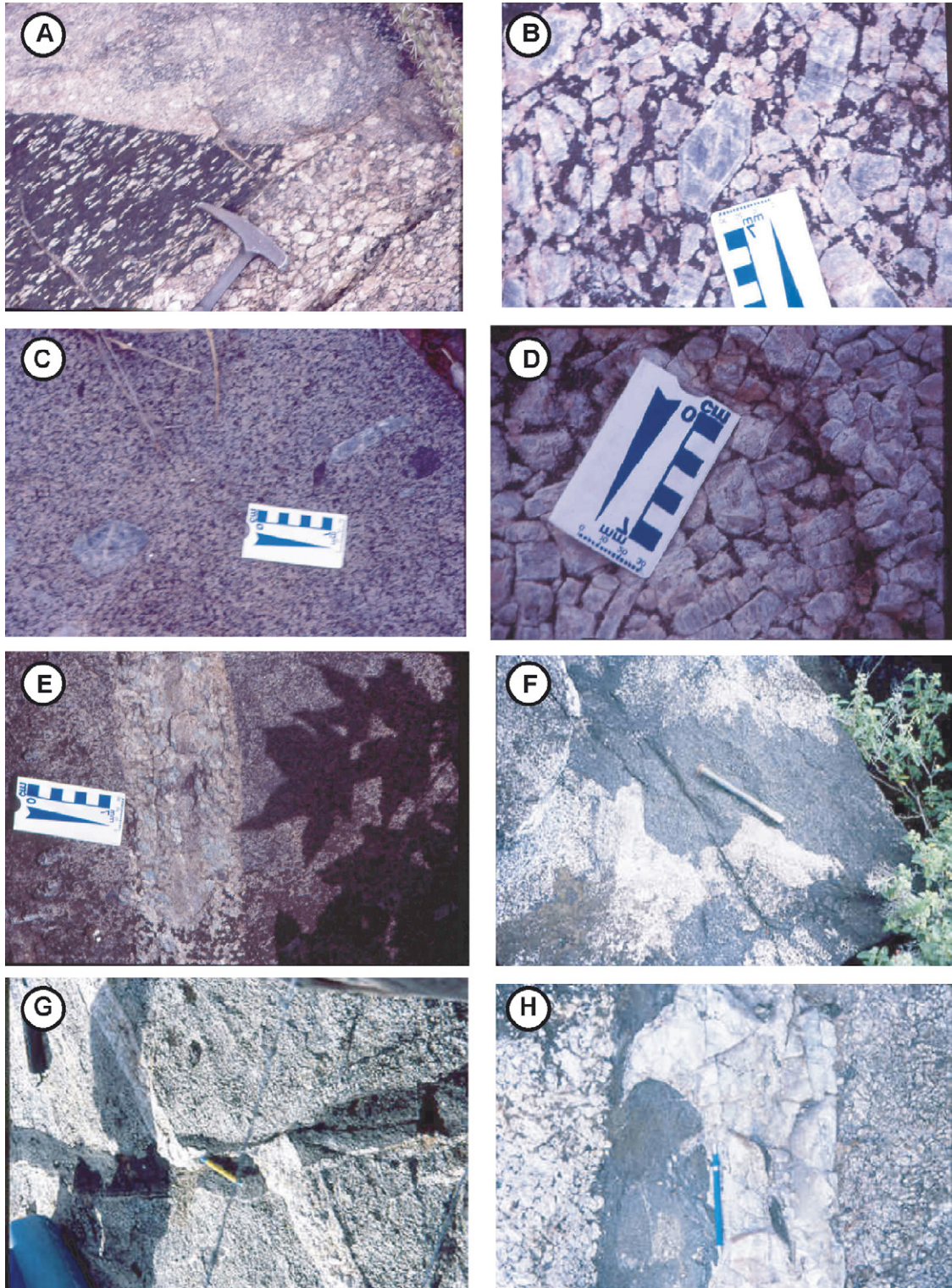
Fig. 3. Field photographs of samples from Morro do Afonso rocks. (A) Fragments of felsic and mafic syenite at the orthoclase-cumulate facies; (B) euhedral zoned phenocrysts of alkali feldspar at the mafic syenite facies; (C) phenocrysts poor sample from felsic syenite; (D) typical field aspect of orthoclase-cumulate facies; (E) amazonite pegmatite dike crosscutting felsic syenite; (F) interfingering relations between lamprophyre and syenite magmas; (G) lamprophyre dike cross cut by quartz pegmatite dike; (H) late quartz dike placed at the same conduit of early lamprophyre magmas.

(Table 1). Diopside crystals are twinned and zoned, with many inclusions of early accessory minerals and borders reacted to amphibole.

Contacts between mafic and felsic syenite are irregular, occasionally globular, showing assimilation of alkali feldspar xenocrysts. Contacts with the feldspar-rich cumulate syenite are sharp with centimeter-wide chilled margins. Mafic autoliths are also present, showing angular shapes similar to the ones described by Blake and Koyaguchi (1991) as a result of interaction between magmas with similar viscosities.

Lamprophyre dykes crosscut the syenite, showing both sharp (Fig. 3E), chilled margins; transitional, commonly irregular, aphanitic borders that grade into strongly porphyritic, locally flow-textured interiors (Fig. 3F). A massive sulphide body has been identified in the southwestern area of MASP, and is probably related to lamprophyric magma (see Rios, 1998, 2002; Plá Cid et al., 2006). The youngest intrusive rocks are represented by numerous quartz pegmatites, some showing large (up to 5 cm) amazonite crystals (Fig. 3E) and aplitic dykes with carbonate, which sometimes show parallelism and occupy the same structural controls as the lamprophyre dykes (Fig. 3G).

At MASP there is no evidence of ductile deformation or structures that can be correlated with the ones observed in basement rocks. The main textures observed are due to magmatic flow during crystallization, which is responsible for most igneous foliations preserved in this intrusion (Figs. 2B and 3A). These structures also comprise igneous layering of mafic cumulate, forming *schlieren* and enclaves, and centimeter-thick mineral layers mainly observed in the mafic syenite.

The petrographic features of MASP rocks are summarized in Fig. 4. According to the modal classification of Streckeisen (1976) the composition of Morro do Afonso intrusion ranges from alkali feldspar syenite to alkali feldspar granite.

4.1. Felsic syenite

The felsic syenite phases are pinkish-grey rocks and form the dominant facies. They are very heterogeneous in terms of mineral assemblage, modal composition and textural relations. The amount of alkali feldspar (orthoclase) phenocrysts ranges from 0 to 60% (Fig. 3A and C), and crystal sizes vary from 0.5 to 5 cm, with some up to 15 cm in length. Most crystals show Carlsbad or Pericline twining, are euhedral, pertitic, prismatic, tabular shaped, and zoned. Other major minerals include diopside (up to 3.3 mm) partially transformed to amphibole (hornblende), and brown biotite (up to 1.2 mm). Syn-

Table 1
Selected petrographic modal analyses of Morro do Afonso Syenite Pluton

|	Mafic syenites							Lamprophyres							Felsic syenites											Cumulate
	1282	939	1266	959	957	1252	932	1281	1264	1322	962	952	953	941	949	958	940	1251	942	1289	961	1317	946	1261	948
Phenocrysts (%)	15	15	25	35	25	40	60	25	30	20	35	20	45	30	35	35	30	60	40	30	40	10	40	20	80
Alkali feldspar	44	63	40	71	–	70	50	20	80	70	86	–	73	100	100	100	100	75	65	100	43	80	80	25	75
Albite																					57	–	–	25	
Diopside	56	37	44	29	80	30	25	–	15	30	–	–	–	–	–	–	–	–	–	–	–	–	–	–	9
Mica	–	–	–	–	20	–	17	–	5	–	–	–	–	–	–	–	–	25	35	–	–	5	–	–	10
Hornblende	–	–	16	–	–	–	8	80	–	–	14	100	27	–	–	–	–			–	–	15	20	50	6
Groundmass (%)	85	85	75	65	75	60	40	75	70	80	65	80	55	70	65	65	70	40	60	70	60	90	60	80	20
Alkali feldspar	30	38	35	5	45	25	35	18	15	8	16	18	20	45	28	23	24	50	43	30	10	35	25	30	7
Diopside	15	30	10	27	13	21	25	18	40	50	20	30	–	15	24	–	6	–	5	–	1	–	–	–	17
Hornblende	20	5	10	–	–	–	18	5	–	20	35	45	60	12	15	33	24	30	8	40	17	16	31	18	5
Mica	20	15	15	18	15	30	18	27	30	14	13	–	5	20	5	19	18	10	1	5	17	25	18	10	12
Plagioclase	5	7	24	45	25	10	15	21	–	–	10	–	5	5	18	12	21	5	22	10	30	12	13	35	48
Quartz	–	–	–	–	–	2	–	–	–	–	2	–	3		5	–	–	2	15	13	10	3	3	5	2
Opaque minerals	4	3	2	4	–	5	2	4	10	4	1	2	3	2	2	9	5	1	1	1	5	2	3	–	5
Accessories	6	2	4	1	2	7	4	7	5	4	3	3	4	1	3	4	2	1	3	1	10	7	7	2	4
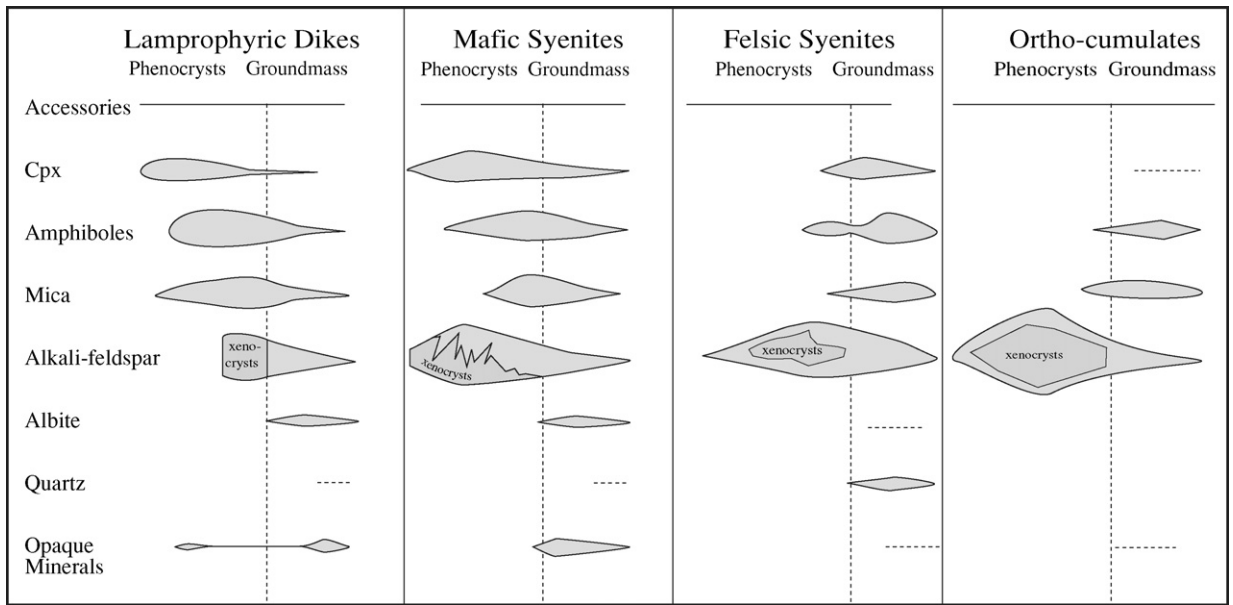
Fig. 4. Schematic representation of modal composition of different petrographic facies at MASP. Xenocrysts refer to the abundance of alkaline feldspar fragments present in the distinct facies.

neusis and epitaxial development over early fragments of alkali feldspar are also observed. Green amphibole phenocrysts (0.4–2.1 cm) are present (Table 1), containing clinopyroxene, apatite, zircon, biotite, and Fe–Ti oxide inclusions, and occasionally show clinopyroxene cores. The leuco-to-mesocratic, fine-to-medium-coarse groundmass of the felsic syenite is made up of almost the same mineral phases (Fig. 4) present as phenocrysts. Small quantities of diopside, mica, quartz, albite and microcline occur along the contacts between the alkali feldspar phenocrysts. Flame-type albite twins and minor undulatory extinction in the anhedral quartz indicate some deformation during crystallization which could mean that the pluton is not entirely post-tectonic. The main accessory phases (Table 1) are zircon, apatite (up to 0.4 mm), titanite, allanite, monazite, and Fe–Ti oxides (pyrite, magnetite, pyrrhotite). Pistacite, chlorite, and carbonate are secondary phases.

A characteristic feature of the felsic syenite is the very strong development of a primary igneous flow lamination, which is defined by the alignment of feldspar phenocrysts. These rocks also exhibit centimetric accumulations of mafic minerals, pillow-like textures, and emulsion figures, suggesting a mingling process. Syn-plutonic dikes and mafic enclaves are common and abundant in particular where emulsion textures are present. The described features are frequently interpreted as produced by co-mingling between mafic and felsic magmas (Barbarin, 1991; Fernandez and Barbarin, 1991,

and references therein), in this case between lamprophyric and syenitic liquids.

4.2. Mafic syenite

The dark gray, mesocratic, mafic syenite phases are found near the pluton borders. A less abundant type (Fig. 2A), they exhibit rounded, gradational, or abrupt contacts and sometimes occur as layers, as darker fine-grained enclaves displaying mingling relationships with their lighter host, or, in some cases, may represent pipes through which the mafic magmas rose.

This facies is characterized by an abundance of mafic enclaves (lamprophyres and autoliths), syn-plutonic (syenite) and late (quartz-feldspar pegmatite) dikes, and shows strong magmatic flow foliation (Fig. 3B). Mineralogy and textures are very similar to those of the felsic syenite (Fig. 4).

Normally, mafic syenite shows lower amounts of phenocrysts than the felsic facies (Table 1). Its subhedral alkali feldspars (0.5–4 cm) are gray in color, and show abundant inclusions of diopside, Fe–Ti oxides, and mica. They are perthitic with Carlsbad twinning, multiple zoning, undulatory extinction, and usually show several intra-crystalline fractures. Broken alkali feldspar phenocrysts show microcline and albite aggregates at their borders. A second generation of phenocrysts is also present, consisting of millimetric crystals of diopside (1.8–2.4 mm), amphibole (1.3–3.7 mm), and mica

(1.2–1.6 mm), although not necessarily associated with each other. Euhedral to subhedral diopside predominates, and is partially transformed to hornblende at the borders. Green hornblende phenocrysts are anhedral to subhedral and sometimes twinned and/or fractured. Biotite phenocrysts are frequently twinned and arranged as aggregates with zircon and apatite inclusions, and mica also develops near the diopside contacts.

The groundmass of mafic syenite is composed primarily of perthitic alkali feldspar, diopside, hornblende, albite-oligoclase, Fe–Ti oxides, titanite, plus accessory phases such as quartz, apatite, zircon, allanite, and occasionally monazite (Fig. 4; Table 1). Carbonate and pistacite are the dominant secondary phases.

4.3. Orthoclase-cumulate

The orthoclase-cumulate phases form (Fig. 2A) topographic elevations in the field. They constitute a monotonous and homogeneous leucocratic facies that makes up almost 12% of the pluton (Fig. 3D). The rocks are pink gray, isotropic, and locally show magmatic flow structures due to alignment of alkali feldspar phenocrysts. Parallel mafic layers occur (0.5–10 m long and <15 cm large). These structures also occur in other syenite bodies of SFC and have been interpreted as flow cumulate features (Conceição, 1990). They typically consist of 80–95% pink, hypersolvus, euhedral to subhedral orthoclase megacrysts (1–10 cm range, 6–8 cm average), with intense zoning that can easily be seen in hand specimen. Orthoclase megacrysts are perthitic, with Carlsbad and Manebach-Pericline twins, and most seem to have grown from early crystal fragments, also of zoned alkali feldspar. Inclusions of diopside and biotite are systematically concentrated near the borders of the crystals.

The groundmass represents less than 20% of these rocks and is dominantly made up of mafic minerals (amphibole > biotite > clinopyroxene), and also small amounts of alkali feldspar, albite and quartz (<2 vol.%). Accessory phases include apatite, titanite, zircon, and subordinately allanite and monazite (Fig. 4; Table 1).

4.4. Lamprophyre

Lamprophyric rocks occur as dikes (Fig. 3G), generally less than 0.5 m wide, although larger dikes (>50 m wide) were also identified. They also occur in the syenitic facies as mafic microgranular enclaves with round, elliptic and angular shapes, and a widespread distribution. Occasionally, structures such as pillows and other features suggesting liquid immiscibility between lamprophyre and syenite were observed.

Two varieties of lamprophyres can be distinguished according to mineral compositions (Rock et al., 1991): minette (only sample 1264) and voguesite (Table 1). Alkali feldspar xenocrysts (2–10 cm) from the syenite have been observed locally. Multiple zoning is usually interrupted, suggesting that they represent fragments of crystals. They also show glomeroporphyritic textures, corrosion-like contacts and are preferentially located at the borders of the dikes. None have been observed in the central parts of the widest dykes. Lamprophyres also contain phenocrysts of diopside (1.5–3.6 mm, up to 1 cm), edenite-hornblende (1.4–3.9 mm, up to 1.5 cm), and Mg-biotite, up to 50 mm in length (Table 1). These phenocrysts are engulfed by a groundmass of similar mineralogy (amphibole–clinopyroxene–mica) together with small amounts of alkali feldspar, albite-oligoclase, Fe–Ti oxides and commonly quartz. Accessory phases are euhedral crystals of zircon, apatite, titanite, allanite and carbonate. For more details on the lamprophyre see Plá Cid et al. (2006).

5. Pb–Pb zircon evaporation ages

Individual zircon grains from two syenite samples were dated. Sample 949 is a felsic syenite, located near the western margin of MASP. Sample 932 is a mafic syenite from the south-central part of the massif (Fig. 2A).

$^{207}Pb/^{206}Pb$ ages obtained with this methodology are interpreted as minimum ages since the degree of discordance cannot be determined. Using Köber methodology the first evaporation steps commonly gave younger ages than at higher temperatures due either to core-overgrowth relationships or mixing of weakly held Pb from damaged crystal domains (Köber, 1986, 1987). The latter explanation is most probable for the MASP data because: (i) increasing zircon age is accompanied by a reduction of $^{204}Pb/^{206}Pb$ ratio (Table 2) indicating that the low temperature deposits contain a larger portion of common lead, which could be derived from altered domains and fractures; (ii) there is no obvious change in radiogenic $^{208}Pb/^{206}Pb$ ratios between the evaporation–deposit cycles as might be expected if zircon growth occurred at two distinct times in different environments; (iii) core-overgrowth relationships were rarely observed under the microscope for the dated crystals.

Sample 949 yielded pale brown to pink zircon crystals, clear to translucid, subhedral to anhedral, ranging in size from 0.05 to 0.15 mm, some with structures that could be cores (Fig. 5), others showing rounded to oval shapes, but mainly prismatic. Fractures and metamict

Table 2
Pb–Pb evaporation on single zircon data for Morro do Afonso felsic and mafic syenite

Zircon number	Evaporation step	Valid blocks	^{204}Pb/^{206}Pb	1σ	^{208}Pb/^{206}Pb	1σ	^{207}Pb/^{206}Pb	1σ	(^{207}Pb/^{206}Pb)c	1σ	Age (^{207}Pb/^{206}Pb) (Ma)	1σ
Felsic syenite, 949 (2098 ± 4 Ma, Finnigan Mass Spectrometer)												
949/1	1	2	0.000252	8	0.3673	13	0.1317	2	0.1283	3	2075	3
949/2	1[a]	0	0.000021	7	0.1117	2	0.1794	5	0.1788	5	2642	5
	2[a]	0	0.000008	0	0.1122	9	0.1782	6	0.1781	6	2635	6
	3[a]	0	0.000088	4	0.1383	2	0.1799	2	0.1788	2	2642	2
949/3	1[b]	0	0.001480	32	0.4022	5	0.1503	1	0.1310	4	2111	6
949/4	1[a]	0	0.001073	21	0.3148	8	0.1357	1	0.1216	3	1981	5
	2[a]	0	0.000248	16	0.3028	44	0.1295	7	0.1262	10	2045	13
	3	1	0.000075	6	0.2778	7	0.1314	3	0.1304	3	2103	4
949/6	1[a]	0	0.000987	5	0.2555	5	0.1410	2	0.1280	2	2071	3
	2	9	0.000883	2	0.2580	6	0.1427	2	0.1311	2	2114	3
	3	10	0.000193	2	0.2385	6	0.1326	1	0.1300	1	2099	1
	4	3	0.000270	1	0.2281	4	0.1332	2	0.1296	2	2093	2
Mafic syenite 932 (2081 ± 13 Ma, VG-354 Mass Spectrometer)												
932/1	1	18	0.000331	51			0.1328	7	0.1302	6	2101	8
932/3	1	6	0.000694	46			0.1358	10	0.1278	15	2068	21
932/4	1	19	0.000365	33			0.1324	4	0.1275	6	2064	8
932/6	1[b]	0	0.001300	247			0.1235	72	0.1058	81	1728	141

[a] Manually eliminated step.
[b] Automatically eliminated step due to high ^{204}Pb.
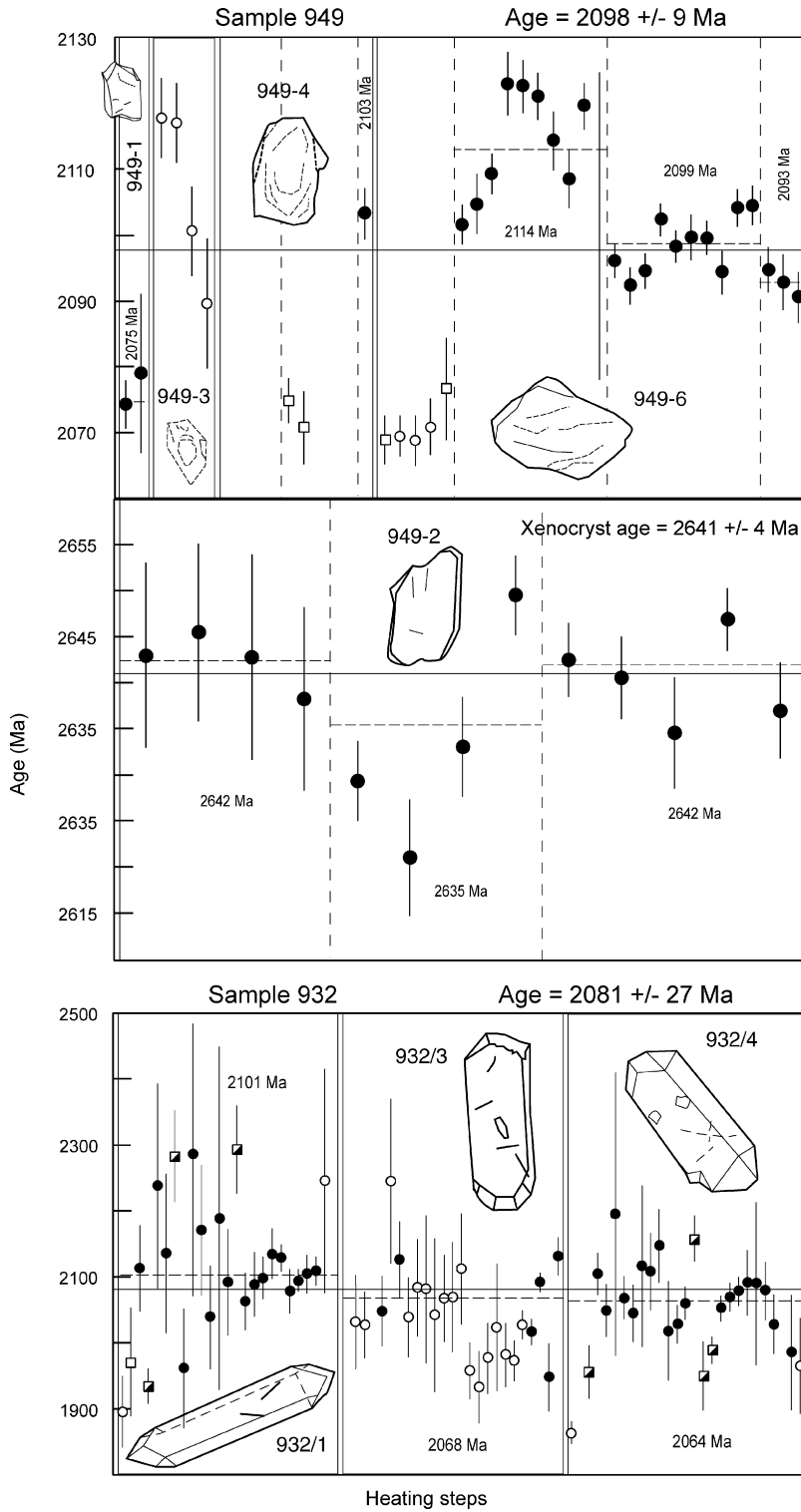
Fig. 5. Age vs. heating steps for evaporation of Pb in zircon grains from samples 949 and 932, Morro do Afonso Syenitic Pluton. Bars represent two sigma errors. Symbols: (●) valid blocks; (○) rejected blocks due to high ^{206}Pb/^{204}Pb ratios (>0.001); (□) rejected blocks due to large 2σ variation, higher than crystal media; (◪) manual rejected blocks due to variations at ^{207}Pb/^{206}Pb ratios. Numbers refer to individual zircon grains. Horizontal lines indicate the mean age of analyzed sample. Dashed lines represent the mean age of analyzed crystal.

areas are common. Inclusions are rare to absent. Three of the analyzed single zircon crystals gave maximum ages that are within analytical error of each other (Fig. 5; Table 2), resulting in an average age of 2098 ± 9 Ma.

An oval-shaped, possibly resorbed, zircon grain gave a $^{207}Pb/^{206}Pb$ age of 2641 ± 4 Ma (Fig. 5; Table 2). This pre-emplacement age indicates the presence of inherited zircon that could be related to contamination of syenite magma during emplacement in Neoarchean basement or from magma source rocks at deeper levels. In either case, Archean rocks this young are still not recorded in SerN (see Rios et al., 2003, 2004).

Sample 932 yielded zircon crystals that are euhedral, elongated (3:1 on average), pink, and have no visible inherited cores. Some of them have a prismatic shape with slightly rounded edges. Three of the dated single zircon crystals gave maximum ages that are within analytical error of each other (Fig. 5; Table 2), resulting in an average age of 2081 ± 13 Ma.

6. U–Pb shrimp zircon ages

SHRIMP methodology was applied to two MASP samples trying to solve the questions related with the apparently too old Pb evaporation ages proposed for this late-orogenic syenites. Zircon concentration and selection were performed at the Jack Satterly Geochronological Laboratory (University of Toronto). Once selected, the zircons were transferred by tweezers to the surface of a piece of sticky tape (3M 666) located on the bottom of a custom Teflon mounting assembly, together with a few fragments of the standard zircon (BR266). Following polishing, the zircons grains were photographed in transmitted and reflected light, coated with high purity Au, and imaged with a scanning electron microscope using back-scattered electron (BSE) detectors (Fig. 6A), to detect cores, rims and other complexities not observable with visible light, which might be present, and to ensure no areas of mixed age were analyzed. These images were used to locate suitable areas for analysis. Common-Pb corrected ratios and ages are reported with a 2σ analytical errors in Table 3. Data are plotted in a concordia diagram with errors at the 2σ level (Fig. 6B).

Sample 961 is a felsic syenite located in the north-central part of the massif (Fig. 2A). Zircons from this sample are pale brown to pink, subhedral, clearly magmatic and the high U or metamitic zones could be avoided when choosing a spot to analyze. The five analyses plot in an array near concordia and a weighted mean calculated from the radiogenic $^{207}Pb/^{206}Pb$ ratios gives an age of 2111 ± 13 Ma (n = 5; MSWD = 1.25; probabil-

Table 3
U–Pb SHRIMP II isotopic data on zircon from Morro do Afonso Syenitic Pluton

| Zircon no.	Analysis no.	U (ppm)	Th (ppm)	$^{232}Th/^{238}U$	$^{204}Pb/^{206}Pb$	$^{206}Pb/^{238}U$	2σ	$^{207}Pb/^{235}U$	2σ	$^{207}Pb/^{206}Pb$	2σ	Disc. (%)	Corr. coeff.
NS 948 (orthoclase-cumulate syenite)													
1	9058-5.1	461	23	0.05	0.000012	0.4044	0.0067	7.32	0.13	2116	8	−3	.963
2	9058-2.1	343	258	0.78	0.000007	0.3816	0.0064	6.91	0.12	2116	10	2	.951
3	9058-7.1	381	286	0.78	0.000114	0.3867	0.0069	6.94	0.13	2100	10	0	.951
4	9058-3.1	240	6	0.03	0.000088	0.3817	0.0085	6.84	0.16	2098	15	1	.937
NS 961 (felsic syenite)													
1	9059-1.1	557	550	1.02	0.001041	0.3762	0.0062	6.86	0.14	2127	20	3	.827
2	9059-5.1	614	596	1.00	0.000296	0.4040	0.0066	7.35	0.13	2124	10	−3	.943
3	9059-7.2	327	225	0.71	0.000127	0.3689	0.0062	6.62	0.12	2100	13	4	.917
4	9059-7.1	566	555	1.01	0.002054	0.4266	0.0070	7.65	0.19	2098	32	−8	.675
5	9059-3.1	370	224	0.63	0.000209	0.3747	0.0063	6.68	0.13	2089	16	2	.875
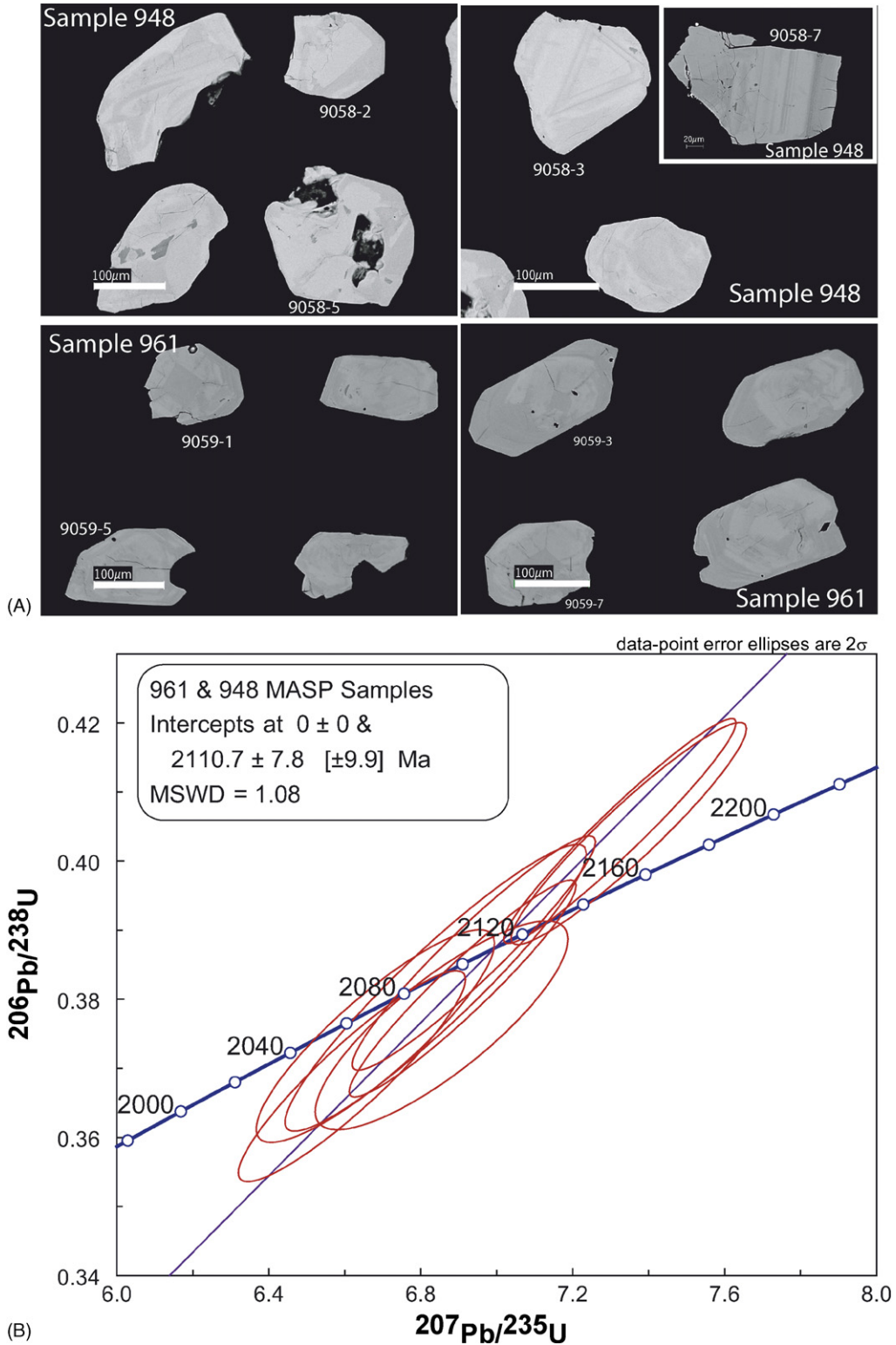
Fig. 6. (A) Back-scattered electron (BSE) scanning electron microscope (SEM) images of representative zircons from the orthoclase-cumulate (sample 948) and felsic syenite (sample 961) analyzed using the SHRIMP. Labels on the photos refer to SHRIMP analyses listed in data (Table 3). (B) U–Pb Concordia diagram of SHRIMP II analyses for samples 948 and 961, with error ellipses at 2σ.

ity = 0.29). Although there were structures suggesting cores, no older ages were found in this sample.

Sample 948 is an orthoclase-cumulate syenite from the western margin of MASP. It yielded zircon crystals that are anhedral, colorless to pink, and have no visible inherited cores. Four analyses of single zircon crystals gave ages that are within analytical error of the ones from sample 961 (Fig. 6; Table 3), resulting in an concordia age of 2111 ± 13 Ma ($n = 4$; MSWD = 1.8; probability = 0.63).

All ages calculations and statistical assessments of the data were processed using the geochronological software package Isoplot/Ex (2.00) of Ludwig (1999). As the samples yields statistical evidence of being a single population of ages, all the nine grains SHRIMP analyses for MASP samples were plotted in the same concordia diagram (Fig. 6B). The weighted mean $^{207}Pb/^{206}Pb$ age of 2111 ± 10 Ma (Fig. 6B) is considered to be the most reliable age estimate for the emplacement of this syenite.

7. Geochemistry

7.1. Major and trace elements

Twenty-one whole rock chemical analyses are presented in Table 4. It is observed that mafic and felsic syenite phases are remarkably similar with respect to their major and trace element geochemistry in spite of clear petrographic criteria that allow them to be discriminated. This is probably because both facies have a similar meso to melanocratic groundmass but differ in the nature and abundance of phenocrysts. Thus, these facies will here be called the "syenite unit" and discussed together although they are identified as distinct symbols on diagrams.

Silica contents of these syenite samples show a small variation, ranging from 53.7 to 64.2 wt.%. Normative compositions (Table 4) and the TAS diagram (Fig. 7) suggest that these rocks are close to the boundary between silica under- and over-saturation, with some samples being nepheline-normative (941, 958, 940, 1266, 1252, 959; Table 4).

Chemically most samples can be classified as syenite or syenodiorite (Fig. 7). MASP rocks belong to the alkaline series, with high contents of alkalis (4.1 wt.% < $Na_2O + K_2O$ < 11.1 wt.%) and, according to the Foley et al. (1987) criteria, can be classified as potassic–ultrapotassic rocks with $K_2O > 4.7$ wt.%; $Na_2O + K_2O$ (7.9–11.1 wt.%); $FeO_T/(FeO_T + MgO) = 0.52–0.75$ and $K_2O/Na_2O = 1.0–2.6$ (Table 4; Fig. 8). The mafic and felsic syenite exhibit a decrease of potassic character (K_2O/Na_2O) with silica enrichment, which is opposite
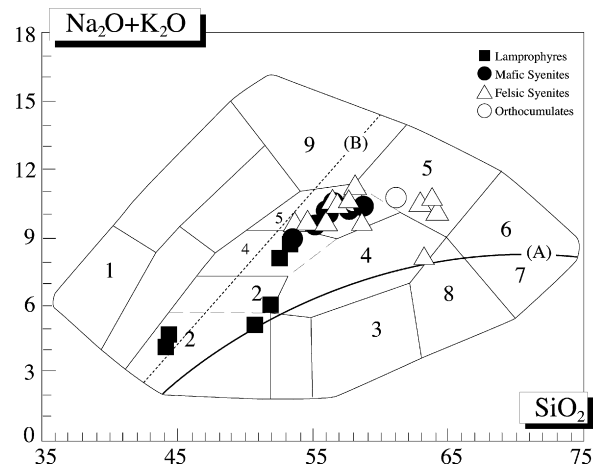
Fig. 7. Alkalis vs. SiO_2 diagram as proposed by Cox et al. (1979) for chemical classification of igneous rocks, with fields for plutonic rocks from Wilson (1989), applied to MASP samples. (1) Ijolite, (2) gabro, (3) diorite, (4) sienodiorite, (5) syenite, (6) alkaline granite, (7) granite, (8) quartz diorite, (9) nepheline syenite. Dashed line correspond to the limits proposed by Irvine and Baragar (1971) to separate alkaline from sub-alkaline rocks. Full line represents the limits between rocks with high and medium alkalinity, as proposed by Schwarzar and Rogers (1974).

to the relationship usually observed between K and Na during magmatic differentiation (Table 4), however, both mafic and felsic syenite show total-alkali enrichment with differentiation.

The agpaitic index between 0.76 and 0.96 points to the metaluminous character ($Al_2O_3/[Na_2O + K_2O] = 1.33–1.80$; $Al_2O_3/[CaO + Na_2O + K_2O] = 0.87–1.38$) of the syenite. P_2O_5 contents are high, with a compatible behavior similar to that observed in TiO_2 (Table 4),

Fig. 8. Composition of potassic to ultrapotassic rocks after Bergman (1987), applied for MASP samples.

Table 4
Chemical compositions and some chemical parameters for rocks from Morro do Afonso Syenite Pluton

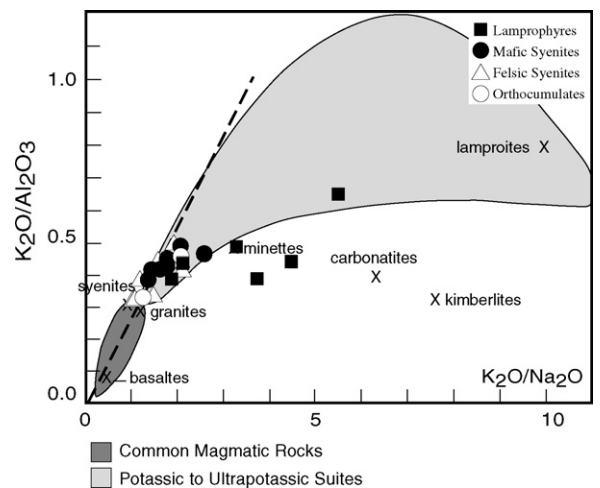| Sample	Felsic syenites											
	941	949	771	958	940	1251	942	1289	961	1317	946	1261
SiO_2 (wt.%)	53.8	54.7	55.92	56.6	56.9	57.7	58.2	59.2	63.2	63.4	63.7	64.2
TiO_2	0.97	0.91	0.83	0.79	0.79	0.85	0.69	0.63	0.44	0.62	0.49	0.52
Al_2O_3	13.8	14.6	14.18	14.6	14.0	14.9	15.5	15.4	16.8	14.2	15.3	16.1
Fe_2O_3	5.0	4.8	6.6	3.8	3.0	3.6	4.3	2.3	1.5	1.6	1.6	1.5
FeO	3.7	3.8	0.0	2.7	3.3	3.0	2.5	2.8	2.3	2.8	2.8	2.1
FeOT	8.2	8.12	5.94	6.12	6.0	6.24	6.37	4.87	3.65	4.24	4.24	3.45
Fe_2O_3T	9.11	9.02	6.6	6.8	6.67	6.93	7.08	5.41	4.06	4.71	4.71	3.83
MnO	0.14	0.14	0.074	0.13	0.12	0.13	0.13	0.21	0.1	0.09	0.13	0.08
MgO	4.4	3.5	2.81	3.3	3.6	3.4	2.2	2.9	1.3	3.9	1.4	1.5
CaO	5.9	4.6	3.97	4.7	5.0	4.4	3.1	5.2	2.2	2.8	2.1	2.4
Na_2O	3.4	3.1	3.48	3.7	3.6	3.5	4.3	3.0	5.1	3.2	4.9	5.0
K_2O	6.1	6.4	6.14	6.8	6.9	6.7	6.8	6.3	5.3	4.7	5.8	5.1
P_2O_5	0.82	0.86	3.48	0.74	0.72	0.65	0.48	0.47	0.23	0.47	0.28	0.25
F						0.14		0.13		0.22		0.089
CO_2						0.16						0.19
S						0.02		0.01		0.01		0.01
H_2Op	0.66	0.65		0.61	0.48	0.2	0.81		0.33		0.76	0.52
Total	98.69	98.06	97.48	98.47	98.41	99.35	99.01	98.55	98.8	98.01	99.26	99.55
Nb (ppm)	25	8		16	15	21	15	10	17	5	19	15
Y	29	30		30	36	31	21	26	13	10	22	14
Zr	620	883		399	306	408	756	12	454	33	592	496
Rb	168	159		200	204	194	188	123	120	161	213	129
Sr	1749	2685		1826	1729	1513	1468	1826	1556	1410	1191	1514
Ba	5246	5820		4572	4591	4178	3603	4362	2978	2884	2827	2824
Th	62	17		36	22	20	40	13	27	26	93	44
Hf	17	18		9	8	9	16		10	8	12	11
V	128	109		104	103	96	75		42		47	47
Cs	17	18		9	8	20	16	16	10	6	12	7
Cr	182	145	56	136	109	143	109		436		75	69
Co	35	25		26	29	49	23		12		11	40
Pb			128			130						107
Ni	65	81		70	49	78	59		124		54	52
Cu	74	26	47	37	30	26	48		30		33	12
Ga	14	17		13	13		17	30	17		19	
Be						4						3
B						38						16
Cl	218	34		86	65		46	30	101	20	140	
Mo						11						
As						17						1
Ag						2						1

Table 4 (*Continued*)

Sample	Felsic syenites											
	941	949	771	958	940	1251	942	1289	961	1317	946	1261
La (ppm)	101.6	130.6		117.6	122.8		99.53		60.59	77.58	113.6	
Ce	225.2	300.5		236.3	262.2		210.2		119.8	159.7	235.1	
Nd	127.3	160.4		101.6	112.1		101.3		56.53	57.85	103.4	
Sm	21.03	25.4		17.72	20.01		16.2		8702	9.24	15.87	
Eu	3.99	4807		3642	4099		3146		2257	1998	1638	
Gd	11.25	12.88		11.78	11.95		8792		4755	5403	8331	
Dy	7123	7109		7.25	7595		5454		2.85	2522	5132	
Ho	1294	1265		1.25	1.38		0.993		0.517	0.37	0.92	
Er	2.83	2624		3161	3041		2182		1129	0.835	1947	
Yb	1773	1499		1791	1952		1437		0.783	0.5	1214	
Lu	0.212	0.186		0.25	0.224		0.179		0.115	0.07	0.157	
Total REE	503.60	647.27		502.34	547.35		449.41		258.03	316.07	487.31	
A.I.	0.88	0.82	0.87	0.92	0.96	0.87	0.93	0.76	0.84	0.73	0.94	0.85
A.S.I.	0.60	0.71	0.72	0.66	0.62	0.71	0.77	0.72	0.93	0.92	0.84	0.89
La_N/Yb_N	38.68	58.81		44.32	42.46		46.75		52.23	104.73	63.16	
La_N/Sm_N	3.04	3.24		4.18	3.86		3.87		4.38	5.29	4.51	
Eu/Eu^*	0.79	0.81		0.77	0.81		0.81		1.07	0.86	0.44	
mg#	34.9	30.1	32.1	35.0	37.5	35.3	25.7	37.3	26.3	47.9	24.8	30.3
Normative parameters (CIPW)												
Qz		0.82	2.74			1.02	0.51	5.10	6.70	14.31	7.12	9.00
Or	36.81	38.86	37.25	41.10	41.68	40.10	40.96	37.87	31.84	28.20	34.83	30.55
Ab	26.43	26.90	30.17	31.84	29.87	29.93	37.01	25.76	43.77	27.43	42.04	42.79
An	4.41	7.15	5.01	3.16	1.64	5.16	2.91	10.05	7.36	10.60	2.62	6.46
Ne	1.56			0.06	0.65							
Di(Ca)	8.58	4.63	6.34	6.78	8.09	5.46	4.13	5.58	0.99	1.97	2.63	1.72
Di(Mg)	6.78	3.47	5.47	5.46	5.76	4.19	3.49	3.79	0.54	1.38	1.33	1.07
Di(Fe)	0.81	0.70	0.00	0.50	1.60	0.68	0.09	1.35	0.41	0.42	1.23	0.54
Hy(Mg)		5.52	1.74			4.41	2.11	3.58	2.76	8.51	2.22	2.73
Hy(Fe)		1.11				0.71	0.05	1.28	2.07	2.58	2.06	1.38
Fo	3.11			2.08	2.40							
Fa	0.41			0.21	0.73							
Mt	7.40	7.15	0.25	5.63	4.44	5.28	6.35	3.39	2.21	2.35	2.36	2.20
He			6.60					0.00				
Ilm	1.88	1.77		1.53	1.53	1.63	1.34	1.22	0.85	1.19	0.95	1.00
Ap	1.83	1.93		1.65	1.61	1.44	1.07	1.04	0.51	1.04	0.62	0.55
	100.00	100.00	95.58	100.00	100.00	100.00	100.00	100.00	100.00	100.00	100.00	100.00

Table 4 (*Continued*)

Sample	Mafic syenites							Orthocumulates		Lamprophyres					
	1282	939	1266	1252	959	957	932	948	772	1322	1264	952	953	962	1281
SiO_2 (wt.%)	53.7	55.2	56.2	56.2	56.6	56.8	58.7	58.0	61.2	44.3	44.5	50.9	52.0	52.5	53.4
TiO_2	1.2	0.89	0.89	0.91	0.78	0.8	0.67	0.74	0.39	2.3	2.1	1.1	1.00	1.3	1.2
Al_2O_3	14.0	13.1	14.9	14.7	14.9	15.5	15.6	15.5	18.04	5.4	7.4	10.6	11.2	12.7	14.5
Fe_2O_3	3.3	3.3	3.3	3.0	3.6	3.5	2.8	3.2	3.85	6.7	5.1	3.6	4.0	4.0	4.7
FeO	5.3	4.4	3.8	3.8	3.4	3.7	2.8	3.0	0.0	10.7	9.1	5.7	4.7	5.0	4.5
FeOT	8.27	7.37	6.77	6.5	6.64	6.85	5.32	5.88	3.46	16.73	13.69	8.94	8.3	8.6	8.73
Fe_2O_3T	9.19	8.19	7.52	7.22	7.38	7.61	5.91	6.53	3.85	18.59	15.21	9.93	9.22	9.56	9.7
MnO	0.15	0.17	0.14	0.14	0.13	0.16	0.14	0.15	0.071	0.33	0.29	0.19	0.18	0.21	0.15
MgO	4.7	5.0	3.9	3.7	3.3	3.0	2.7	2.4	1.71	10.2	11.4	7.7	6.8	5.1	4.5
CaO	5.5	5.5	4.8	4.7	4.5	3.9	3.7	3.5	2.39	11.8	12.4	10.3	9.5	6.9	5.5
Na_2O	2.5	3.1	3.8	3.7	4.3	3.7	4.4	3.4	4.77	0.64	1.1	1.1	1.1	2.6	3.0
K_2O	6.5	6.4	6.2	6.6	6.2	6.6	6.0	7.1	5.96	3.5	3.6	4.1	4.9	5.5	5.6
P_2O_5	1.1	0.9	0.67	0.7	0.64	0.59	0.47	0.6	0.23	2.1	1.8	1.5	1.5	1.2	1.1
F	0.3		0.19	0.23						0.55	0.43				0.24
CO_2		0.73	0.23	0.56							0.23				
S	0.02		0.01	0.01						0.03	0.02				0.02
H_2Op			0.33		0.68	0.6	0.85	0.95			0.47	0.55	1.06	1.03	
Total	98.27	98.69	99.36	98.95	99.03	98.85	98.83	98.54	98.61	98.55	99.94	97.34	97.94	98.04	98.41
Nb (ppm)	17	9	17	17	11	15	14	11		21	19	11	16	31	12
Y	28	34	28	31	30	20	20	27		72	65	40	41	43	38
Zr	32	173	512	370	568	590	369	206		55	398	352	333	243	23
Rb	167	186	189	193	195	178	153	229		148	149	89	115	175	145
Sr	1688	1714	1458	1554	1623	1457	2039	2476		135	323	1838	2112	1979	1472
Ba	5078	4133	3645	3917	4023	3722	4518	4977		1827	2266	5394	6105	7140	2497
Th	6		37	19	40	56	12			35	8	33	24	12	
Hf		8	12	9	12	15	12	8		13	9				
V		117	101	101	102	85	80	74			242	163	136	142	
Cs	30	8	25	17	12	15	8	8		12	17	5	5	8	10
Cr		473	113	96	100	164	136	173	48		299	209	191	182	
Co		31	48	53	29	28	20	22			73	33	27	30	
Pb			133	126					128		71				
Ni		108	61	54	59	76	65	76			125	86	70	97	
Cu		33	43	22	63	41	41	33	17		64	174	48	100	
Ga		12			16	16	16	13				10	10	10	
Be			6	4							5				
B			20	11							16				
Cl		76			167	40	109	21		440		136	88	62	20
Mo				8							10				
As			8	7							2				
Ag			1	1							2				

Table 4 (*Continued*)

Sample	Mafic syenites							Orthocumulates		Lamprophyres					
	1282	939	1266	1252	959	957	932	948	772	1322	1264	952	953	962	1281
La (ppm)	123.5	95.45			100.3	107.8	65.12	115.5		277.6		193.6	191.2	193.1	140
Ce	288.7	204.7			226.5	233.8	140.1	245.1		582.4		405	424.3	408.5	328.1
Nd	119.1	100.8			98.57	111.6	74.33	127.2		223		185.5	237.1	179.5	123.9
Sm	18.68	16.6			16.77	18.47	12.16	20.13		37.09		36.57	37.76	27.84	21.35
Eu	3769	3237			3.53	3742	2783	4.29		4505		6744	6553	4419	4456
Gd	10.46	9386			10.86	10.67	6685	10.27		22.22		21.89	18.43	17.03	12.4
Dy	4936	5722			7.1	6127	4112	5522		10.05		10.8	8245	8972	5685
Ho	0.74	1061			1232	1106	0.737	0.965		1.61		1895	1398	1689	0.87
Er	1.61	2444			2.81	2379	1.56	1.9		3.35		3702	2509	4024	1.9
Yb	1009	1559			1851	1495	1048	1277		1.71		1766	1082	2132	1114
Lu	0.153	0.197			0.285	0.196	0.126	0.165		0.231		0.148	0.121	0.304	0.165
Total REE	572.66	441.16			469.81	497.38	308.76	532.32		1163.77		867.62	928.70	847.51	639.94
A.I.	0.80	0.92	0.87	0.90	0.93	0.85	0.88	0.86	0.79	0.90	0.77	0.59	0.64	0.81	0.76
A.S.I.	0.66	0.59	0.69	0.67	0.68	0.76	0.76	0.79	0.97	0.20	0.26	0.42	0.46	0.56	0.69
La_N/Yb_N	82.62	41.33			36.58	48.67	41.94	61.05		109.58		74.00	119.28	61.13	84.83
La_N/Sm_N	4.16	3.62			3.77	3.67	3.37	3.61		4.71		3.33	3.19	4.37	4.13
Eu/Eu^*	0.82	0.79			0.80	0.81	0.94	0.91		0.48		0.73	0.76	0.62	0.84
mg#	36.2	40.4	36.6	36.3	33.2	30.5	33.7	29.0	33.1	37.9	45.4	46.3	45.0	37.2	34.0
Normative parameters (CIPW)															
Qz							0.78	2.37	5.67		14.31	2.93	4.29		0.02
Or	39.25	38.64	37.19	39.77	37.29	39.73	36.22	43.03	36.87	21.13	28.20	25.06	29.92	33.53	33.75
Ab	21.57	26.75	32.06	30.25	33.78	31.83	37.95	29.45	42.17	5.52	27.43	9.61	9.60	22.65	25.83
An	7.89	2.94	5.31	4.03	3.04	6.24	5.15	6.15	2.04	1.53	10.60	12.22	11.46	6.90	9.69
Ne			0.28	0.87	1.72										
Di(Ca)	5.59	8.15	6.20	6.49	6.61	4.15	4.50	3.36	3.74	19.06	1.97	13.14	11.74	8.82	4.82
Di(Mg)	3.59	5.60	4.33	4.42	4.74	2.77	3.17	2.33	3.22	12.41	1.38	9.16	8.59	6.11	3.52
Di(Fe)	1.62	1.88	1.35	1.55	1.27	1.06	0.93	0.74		5.31	0.42	2.86	2.02	1.97	0.84
Hy(Mg)	5.03	1.49				3.49	3.72	3.82	1.25	4.93	8.51	10.73	8.96	5.66	7.94
Hy(Fe)	2.26	0.50				1.34	1.09	1.22		2.11	2.58	3.35	2.11	1.83	1.89
Fo	2.36	3.97	3.89	3.50	2.56	0.96				6.08				0.96	
Fa	1.18	1.47	1.34	1.36	0.76	0.41				2.87				0.34	
Mt	4.89	4.88	4.85	4.43	5.31	5.17	4.14	4.75	0.24	9.92	2.35	5.39	5.99	5.98	6.94
He									3.86						
Ilm	2.33	1.73	1.72	1.76	1.51	1.55	1.30	1.44	0.00	4.46	1.19	2.16	1.96	2.55	2.32
Ap	2.45	2.01	1.48	1.56	1.42	1.31	1.05	1.34	0.53	4.68	1.04	3.38	3.38	2.70	2.45
	100.00	100.00	100.00	100.00	100.00	100.00	100.00	100.00	99.59	100.00	100.00	99.99	100.00	100.00	100.00

A.I. (agpaitic index) = molar (Na + K)/Al, mg# = molecular Mg/(Mg + Fe2T), mg## = (MgO/(MgO + FeOt)) × 100 em % peso, A.S.I. (aluminum saturation index) = molar Al_2O_3/(CaO + Na_2O + K_2O), lamproites have K_2O/Al_2O_3 ratio > 0.6 (Foley et al., 1987).

although the low titanium concentrations from MASP indicate depleted rocks.

Lamprophyric rocks are less differentiated ($44\% < SiO_2 < 53\%$, Table 4). The most undersaturated voguesites have been attributed to the less differentiated cumulate samples (Rios, 2002; Plá Cid et al., 2006).

The high MgO (4.5–11.4 wt.%) and K_2O (3.5–5.6 wt.%) contents, as well as the K_2O/Na_2O ratio greater than 2, point to an ultrapotassic composition for the parental liquid (Fig. 8; Foley et al., 1987; Foley and Peccerillo, 1992). These are metaluminous rocks with low to moderate Al_2O_3 contents (5.4–14.5%), but their low Ca contents (CaO = 5.5–12.4%), associated with high K (K_2O = 3.5–5.6%) and Rb (89–175 ppm)

and some other features are diagnostic of lamproites (see Mitchell and Bergman, 1991; Plá Cid et al., 2006).

Harker diagrams show well-defined magmatic trends pointing to fractional crystallization processes dominating the evolution of Morro do Afonso Syenite (Fig. 9). The linearity of lamprophyre with syenite trends for all major elements suggests a genetic relation. Elements such as Ti, Fe, Ca, Mg, and P show compatible behavior, and are probably related to fractionation of Fe–Mg phases, oxides, and apatite. On the other hand, incompatible behavior of Na and Al preclude fractionation of plagioclase and perhaps alkali feldspar, at least up to a 60 wt.% silica level in the magma. Cumulate processes seem to be associated with fractionation, as observed in the less-evolved lamprophyre, which is frequently out of
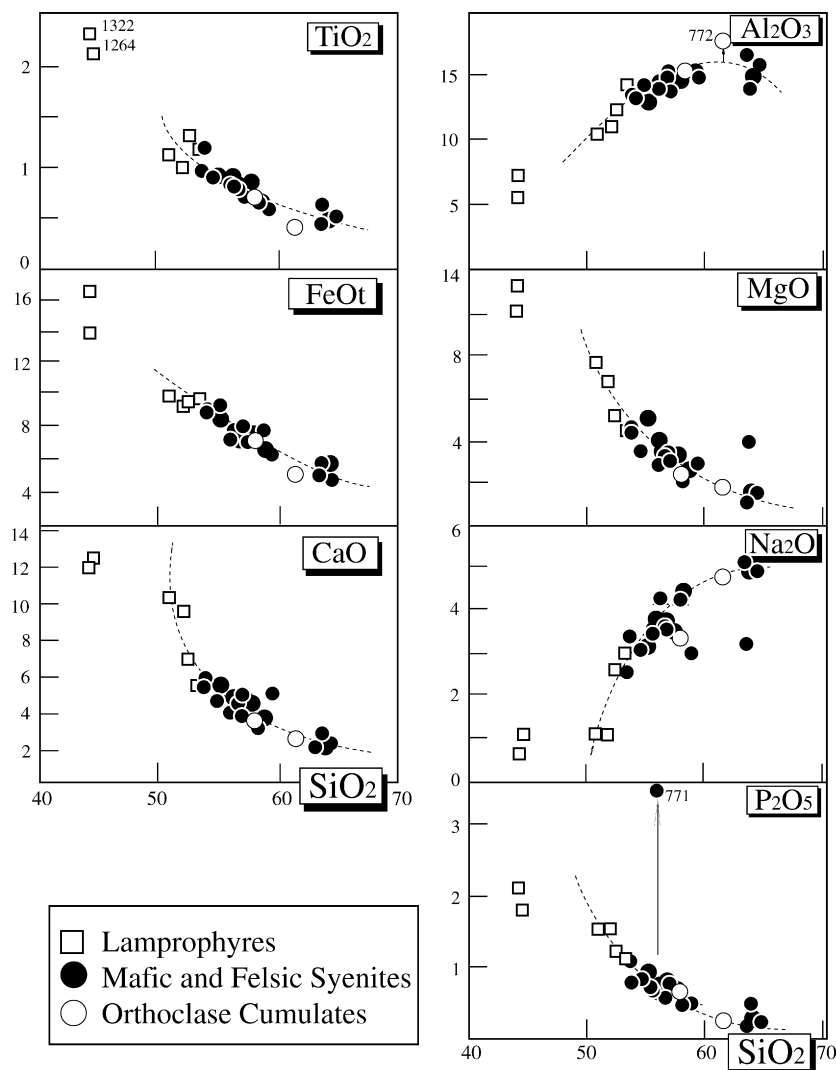
Fig. 9. Major-element Harker diagrams for the MASP suite rocks.

trend for elements such as Ti, Ca, Mg, Na, and P. The very high phosphorous content of syenite sample 771 suggests apatite accumulation.

The syenitic rocks from MASP are extremely enriched in all LIL elements, as mainly observed for the high contents of Ba and Sr, whereas Rb shows moderate concentrations (Fig. 10; Table 4). In addition, the rocks of this suite are depleted in some HFS elements such as Nb, Y and Hf (Fig. 10; Table 4). These characteristics are typically associated with magmas produced by melting of an enriched-mantle rather than a MORB-type source (Pearce and Cann, 1973; Pearce and Norry, 1979; Green, 1980). Such enrichment occurs in the mantle wedge by metasomatism following dehydration of a subducted oceanic slab in the lithospheric mantle. Moderate to low contents of compatible elements such as Cr and Ni are not typical of magmas equilibrated with normal peridotitic or harzburgitic sources, although they suggest derivation from primitive potassic melts.

In Fig. 10, it is possible to observe the geochemical characteristics described above, and the strong similarity with the spatially co-existing lamprophyre. These multi-elementary diagrams indicate a probable co-genetic relationship between syenite and lamprophyre. The more pronounced negative Sr anomalies in lamprophyric rocks are due to the higher contents of LREE, whereas the lower Zr concentrations perhaps reflect the higher alkalinity of lamprophyre magmas. MASP rocks also show a remarkable similarity to the means presented for minette and phlogopite lamproite in the literature (Rock et al., 1991; Mitchell and Bergman, 1991).
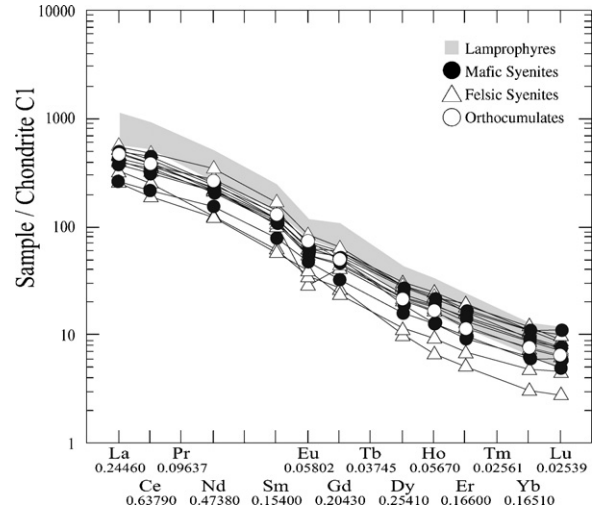
Fig. 11. Rare earth element diagram chondrite-normalized (Evensen et al., 1978) for MASP. Associated lamprophyric rocks in shading.

Fig. 11 shows chondrite-normalized rare earth elements (REE) distribution patterns. All samples (syenite and lamprophyre) are quite similar with parallel slopes. Lamprophyre shows more enriched REE patterns (Table 4), and sample 1332, with a cumulate origin, shows the highest concentrations, mainly of LREE due to the accumulation of apatite as indicated by its extremely high concentrations of P_2O_5. Whole REE contents of syenite are high and extremely fractionated, exhibiting moderate and variable LREE fractionation ($La_N/Sm_N = 3.0–5.3$) and high LREE/HREE ratios ($La_N/Yb_N = 36–105$). Eu-anomalies are slightly
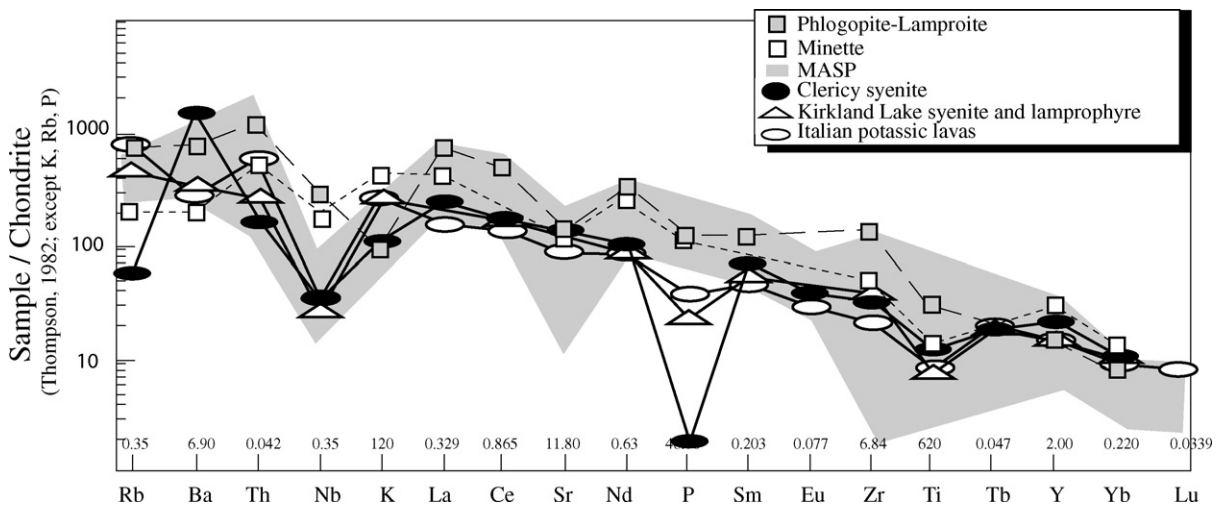
Fig. 10. Trace element concentrations for MASP rocks normalized to the composition of chondrites. The normalizing values are from Thompson (1982). Rb, K and P from primitive mantle values of Sun (1980). Also show is the mean for minnetes (Rock et al., 1991), phlogopite-lamproites (Bergman, 1987), and similar potassic rocks worldwide (Sun, 1980).

negative (Eu/Eu* = 0.77–0.94), except for samples 961 (1.07) and 946 (0.44). Syenite sample 961 shows higher Al_2O_3 concentrations, and also higher amounts of modal albite phenocrysts and Or + Ab + An normative values, which probably reflects a slight feldspar-cumulate component. Lamprophyre shows more negative Eu anomalies (Eu/Eu* = 0.58–0.78). The REE fractionation is probably inherited from the source, requiring that it be metasomatically enriched in LREE prior to melting.

7.2. Sr and Nd isotopic composition

The Sr and Nd initial isotope compositions at 2.1 Ga have been determined from whole rock syenite and lamprophyre samples of MASP (Table 5; Fig. 12). Three Sr analyses are also available for lamprophyric rocks.

The initial $^{87}Sr/^{86}Sr$ and $^{143}Nd/^{144}Nd$ ratios for these syenitic rocks vary within narrow ranges, respectively, 0.7033–0.7042 and 0.509800–0.509805. Such values are relatively low compared to published Sr–Nd isotope analyses of potassic–ultrapotassic rocks worldwide, being comparable to those from West Africa (Peaucat et al., 2005) (see Fig. 12). Nd isotopic data reported in terms of $\varepsilon_{Nd(T)}$ range from −2.36 to −2.80 (Table 5). The Nd T_{DM} model ages are indistinguishable at 2.56 and 2.58 Ga, assuming a two-stage evolution as proposed by De Paolo and Schubert (1991). Details are described in Rios (2002). The Neoarchean model age, along with
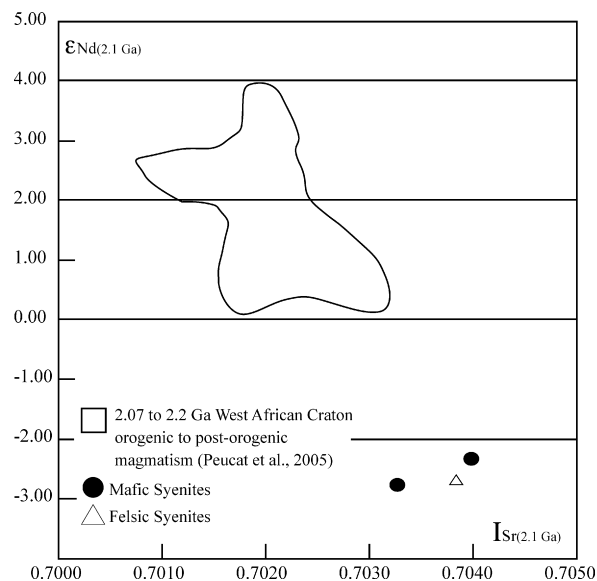
Fig. 12. E_{Nd} vs. initial Sr isotopic variations at 2098 Ma for magmas of MASP. The delimited area represents the 2.07–2.20 Ga West African Craton magmatism (Peucat et al., 2005).

Table 5
Whole rock Rb–Sr and Sm–Nd data for magmatic rocks of the Morro do Afonso Syenite Pluton

Sample no.	Rock	Age (Ma)	Sm (ppm)	Nd (ppm)	$^{143}Nd/^{144}Nd$	$^{147}Sm/^{144}Nd$	T_{chur} (Ga)	T_{DM} (Ga)	$\varepsilon_{Nd(0)}$	$\varepsilon_{Nd(T)}$	$f_{Sm/Nd}$	$(^{147}Sm/^{144}Nd)$am	I_{Nd}	Rb (ppm)	Sr (ppm)	$^{87}Rb/^{86}Sr$	$^{87}Sr/^{86}Sr$	I_{Sr}	$\varepsilon_{Sr(T)}$
953	Lamprophyre	2098												144.00	2501.89	0.1666	0.70838	0.7034	18.65
952	Lamprophyre	2098												139.62	2483.09	0.1627	0.70829	0.7034	19.05
962	Lamprophyre	2098												311.04	2391.94	0.3767	0.71535	0.7041	27.44
942	Felsic syenite	2098												225.36	1534.49	0.4254	0.71665	0.7038	24.98
961	Felsic syenite	2098												135.40	1540.10	0.2546	0.71186	0.7042	30.32
946	Felsic syenite	2098	13.124	85.05	0.511084	0.0933	2.28	2.58	−30.31	−2.70	−0.53	0.09	0.5098	241.46	1287.32	0.5435	0.72013	0.7038	23.68
958	Mafic syenite	2098	20.909	118.11	0.511267	0.1071	2.32	2.58	−26.74	−2.80	−0.46	0.11	0.5098	249.50	1868.09	0.3868	0.71488	0.7033	16.39
957	Mafic syenite	2098	19.893	111.66	0.511289	0.1078	2.30	2.56	−26.31	−2.36	−0.45	0.11	0.5098	235.15	1764.10	0.3861	0.71567	0.7040	27.95

the similarly old inherited zircon crystal, suggests significant involvement of older crustal components in the origin of these rocks. The degree of isotopic enrichment is similar to the rocks described by Doumbia et al. (1998). The Neoarchean signature may be the result of mixing between Meso or Paleoarchean crust and a juvenile 2.1 Ga mantle component.

8. Discussion

8.1. Geochronological implications

Alkaline rocks represent the latest magmatic event in the Serrinha Nucleus and are related to the end of the Transamazonian Orogeny. Field features at MASP reinforce this opinion: only magmatic flux foliations have been observed, although the pegmatitic veins are displaced by E–W fractures. The evidence of included crystal fragments, as well as some corrosion features observed in the orthocumulate facies, suggests transport by magmatic flow and a complex magmatic evolution, probably due to convective movements. The syenite magmatism of SerN, including MASP, is found roughly along the 39° longitude (Fig. 1C). This is interpreted by Rios (2002) to result from a regional tectonic control. It is parallel to a similar large alignment (>1000 km) of four N–S elongated syenite bodies (Itiúba, Santanápolis, São Félix, Anuri) in the nearby Salvador-Curaçá Mobile Belt.

The combined use of Pb evaporation and SHRIMP techniques yielded ages in the range 2.08–2.11 Ga for MASP rocks. However, the age of 2.11 Ga is more than 100 Ma older than previously suggested for the metamorphic peak of Transamazonian Orogeny at São Francisco Craton (2.0 Ga, Barbosa and Sabaté, 2004). These limits were proposed on the basis of Rb–Sr isochrons, Pb–Pb whole rock, Pb–Pb evaporation, and monazites ages. This new U–Pb single zircon age, together with others U–Pb new data for late-tectonic plutons (Conceição et al., 1999, 2002, 2003 and others) reinforce that: (i) Serrinha Nucleus alkaline rocks were emplaced at around 2.1 Ga; (ii) the late-tectonic undeformed Paleoproterozoic syenites at São Francisco Craton are related to the end of Transamazonian Orogeny; (iii) the previous chronology for the metamorphic peak is not valid, been so young.

The Paleoproterozoic alkaline granitoids are not affected by the deformation related to the end of Transamazonian Orogeny and therefore their age of 2.1 Ga set the minimum time for the Transamazonian metamorphic event. Important to note is that the zircons from some of the older granitoids in the area record evidence of a Paleoproterozoic thermo-tectonic event at 2.07 Ga, related with the emplacement of the youngest igneous event at Serrinha Nucleus, the so called Morro do Lopes Granites (Rios et al., 2003, 2005, 2006).

8.2. Regional perspectives

Serrinha Nucleus is one of the largest gold producers in South America. At SerN, ultrapotassic lamprophyre has a close spatial association with syenite (Conceição et al., 1995; Plá Cid et al., 2006), as well as with gold deposits. Many authors have speculated (e.g. Rock and Groves, 1988; Rock et al., 1991) that there is a genetic link between lamprophyre and mesothermal gold, although others (e.g. Wyman and Kerrich, 1989) suggest that lamprophyre magma simply shares the same structural control as mesothermal vein systems. The observed evidence for mixing and mingling can explain the origin and diversity of MASP rocks while the presence of cumulates suggests an important process of in situ differentiation. Lamprophyre is also described at other locations in SerN area, always associated with syenitic rocks although, at the Maria Preta Au-Mine, minette is the most common lamprophyre type described (Barrueto, 1997), whereas in the MASP voguesite is dominant.

MASP consists of rocks derived from ultrapotassic lamprophyre magmas that evolved and/or mixed with a K-syenite liquid (trachyte magma). The ultrapotassic composition of its lamprophyre and mingling textures imply a genetic link with the syenite. This hypothetical relationship is consistent with the Rock et al. (1991) suggestion of a genetic association between calc-alkaline/shoshonitic lamprophyre and the generation of granitoid plutons in orogenic belts. Thus, the alkali feldspar xenocrysts are thought to be fragments derived from syenite xenoliths partially digested by the lamprophyre magma. In fact, metre size syenite xenoliths are abundant in the largest known lamprophyre dyke. Textural and structural relations within MASP suggest the co-existence of lamprophyre and intermediate mafic syenite magmas during different crystallization stages. Locally, lamprophyre crosscuts the syenite cumulates showing sharp contacts and chilled margins (Fig. 3G). Complex interfingering of lamprophyre dikes and syenite as well as the injection of lamprophyre along fine fractures are common. Ultramafic xenoliths are scattered throughout the lamprophyre. However, common evidence for mingling at the contacts between lamprophyre and syenite (Fig. 3F), shows that the two phases co-existed as magmas and crystal mush (see also Conceição et al., 1995; Plá Cid et al., 2006).

Although the most studied suites of ultrapotassic rocks have Phanerozoic ages (Foley et al., 1987; Peccerillo et al., 1984, 1988; Rogers et al., 1985, and references therein), Precambrian ultrapotassic rocks have been reported from Australia and Canada (Atkinson et al., 1984; Corriveau and Gorton, 1993; Wyman and Kerrich, 1989; Bourne and L'Heureux, 1991). In SerN, other syenite plutons located in immediately adjacent portions of Santa Luz City have been dated by Rios (2002). The high precision U–Pb geochronology obtained for the Serra do Pintado Syenite (2098 ± 2 Ma; Conceição et al., 2002; Fig. 1B; 16 km^2) overlaps with the MASP ages at 2.1 Ga, although the Agulhas-Bananas Syenitic Pluton (26 km^2), aged 2086 ± 9 Ma (^{207}Pb/^{206}Pb on zircon; see Conceição et al., 2002), overlaps with the younger ^{207}Pb/^{206}Pb age from MASP. The same is also true for the Itiúba Batholith (Conceição et al., 2003; 2095 ± 5, Pb–Pb, 1800 km^2), Santanápolis Pluton (Conceição et al., 1997; 2100 ± 1 Ma, U–Pb, 180 km^2), São Félix Massif (Rosa et al., 2001; 2098 ± 1, Pb–Pb, 32 km^2), and the Anuri Massif (Conceição et al., 1997; 2098 ± 5 Ma, U–Pb, 70 km^2). Since these syenite plutons share some geochemical features with MASP rocks and are indistinguishable in age, it is not unreasonable to propose that all of these rocks collectively define a 2.1 Ga old potassic–ultrapotassic igneous province in the East São Francisco Craton.

Syenitic rocks located in Western Bahia Province (Rosa et al., 1996, 2000; Guanambi: 2054 ± 8 Ma; Cara Suja: 2053 ± 3 Ma; Estreito: 2054 ± 3 Ma; Ceraíma: 2050 ± 1 Ma; U–Pb) are also indistinguishable in age but are slightly younger than those to the east. Similar petrography, geochemical and isotopic features among all the syenite phases, suggests that this ultrapotassic igneous province occupies a wide area in much of Bahia State.

The timing of gold mineralization in SerN (2.05–2.07 Ga; Vasconcelos and Becker, 1992; Barrueto, 1997; Silva et al., 2001), although not tightly constrained, is comparable to that of ultrapotassic magmatism. The age data, geochemical signatures, and field relationships are permissive of the hypothesis that gold mineralization was related to magmatic fluids that evolved during the emplacement of late to post-tectonic syenite plutons at ca 2.1 Ga.

8.3. Geochemical aspects and nature of the MASP suite

The results of whole rock geochemistry, geochronology, and Sr and Nd isotopic analyses for the syenite discussed above provide some constrains on the origin of these rocks. Major elements display a large variation reflecting the different petrographic characteristics of each intrusive facies: FeO$_T$, MgO, CaO, MnO, TiO$_2$, and P$_2$O$_5$ abundances decrease with increasing differentiation, whereas Al$_2$O$_3$, Na$_2$O and K$_2$O increase along with the silica content up to ∼60 wt.% SiO$_2$, and then decrease. TiO$_2$ contents are low (0.4–1.2%) and Al$_2$O$_3$ contents are variable (13–18 wt.%), which is typical for subduction-related potassic igneous rocks (Peterson et al., 2002).

The ranges of normative compositions (Table 4) and the degrees of enrichment in incompatible elements (both LILE and HFSE) are also considerable: rocks from MASP show LILE enrichment relative to HFSE, with high concentrations of halogens (Cl and F) and volatiles; high potassic character (molar K/Na ratio = 1.0–2.6 for syenite and 1.5–5.5 for lamprophyre), accompanied by strong enrichment in Rb, Ba, and Sr, which increase with the degree of undersaturation; high CaO (up to ∼12%) concentrations as well as low K$_2$O/Al$_2$O$_3$ ratios (0.31–0.64) (see Table 4).

The alkaline potassic to ultrapotassic feature of MASP rocks is shown by the presence of abundant orthoclase phenocrysts. Samples 939, 949, and 1282 fit the full definition of ultrapotassic rocks, following the criteria of Foley et al. (1987): K$_2$O > 3%; MgO > 3%; K$_2$O/Na$_2$O > 2. Two other samples fail to satisfy the required MgO concentrations (1289 = 2.9% and 948 = 2.4%). Although the other syenite samples do not satisfy the K$_2$O/Na$_2$O (1.02–1.92) criterium and are therefore regarded as potassic (Bergman, 1987; Peccerillo, 1992; Müller and Groves, 1995; Fig. 7). Foley et al. (1987) state that the MgO criterium is intended to confine the ultrapotassic definition to rocks that are predominantly of mafic character, which are the lamprophyric rocks in the case of MASP. The lamprophyre associated with the syenite is ultrapotassic regarding all Foley et al. (1987) criteria, but they also show transitional features to lamproite (Plá Cid et al., 2006). A satisfactory model to explain the origin of syenite potassic magmas at SFC should be able to account for the production of a wide spectrum of K-rich melts with peculiar geochemical and isotopic features, i.e. low TiO$_2$, low K$_2$O/Al$_2$O$_3$ and high LILE/HFSE ratios.

8.4. Evidence of a subduction-related origin for MASP enrichment

There are three main groups of models to explain the origin of syenite: (1) melting of crustal rocks (Lubala et al., 1994; Tchameni et al., 2001); (2) partial melting of metasomatized mantle (Sutcliffe et al., 1990; Lynch et

al., 1993); (3) magma mixing processes (Dorais, 1990; Zhao et al., 1995). This diversity reflects the variety of tectonic environments in which they are found, but all geodynamic interpretations of potassic magmatism fall into two main categories which claim either a key role of subduction in mantle enrichment processes (Rogers et al., 1985; Serri et al., 1993) or consider them as an expression of continental rift magmatism (Lavecchia and Stoppa, 1990, 1996). These models depend heavily on the mechanisms proposed to explain the Ti, Nb, Ta anomalies and the LILE enrichment so common in ultrapotassic suites.

MASP syenite falls into the "volcanic arc granites" field on the tectonic discrimination diagrams (not shown) of Pearce et al. (1984), attesting to derivation from sources consistent with a subduction environment. Attempting to better discriminate the tectonic environment of these rocks, the hierarchical set of discrimination diagrams (not shown) for potassic igneous rocks proposed by Müller et al. (1992) were used, confirming that these are orogenic rocks related to subduction. Pearce (1983) suggested that LILE enrichment could be caused by a melt derived from subducted crust that resulted in mantle enrichment. LILE enrichment is a common feature to all Serrinha Nucleus Paleoproterozoic granitoid rocks (Rios, 2002; Conceição et al., 2002) and patterns are similar to those of granitoid rocks emplaced in an active continental margin context (Pearce et al., 1984; Doumbia et al., 1998).

MASP rocks have very low Nb/Zr ratios (0.01–0.53) which differ from intraplate syenite, generally characterized by Nb/Zr ratios > 100 (Fig. 13). Their low Hf/Sm ratios (0.40–1.15) and chondrite-normalized trace element profiles (Fig. 10), are also indicative of subduction-related orogenic alkaline magmas (Laflèche et al., 1991). Peccerillo et al. (1988) suggest that ultrapotassic systems preserve the pattern of their extended trace element plots when passing from mafic to intermediate members during fractional crystallization. Thus,
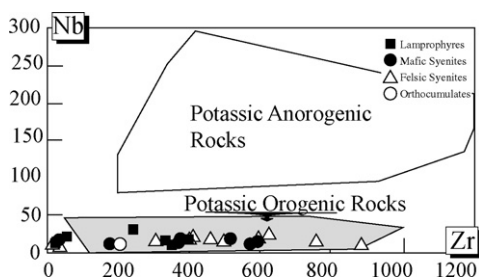
the presence of TiO_2 and Nb anomalies in both syenite and lamprophyre at MASP can be taken as one more evidence in favour of a subduction related origin for the MASP source enrichment.

In magmas with high agpaitic index, such as at MASP, Zr saturates at high concentrations so zircon is a late crystallizing mineral (Watson and Harrison, 1983). Thus, the absence of negative Zr anomalies in syenitic rocks does not rule out their derivation by fractional crystallization from lamprophyre magma. However, although these rocks show a characteristic depletion in HFSE (Ti, P, Nb) relative to LILE (Rb, K, Ba), the high concentrations of Ba, Rb, Th, K, and LREE observed in the trace element diagrams (Fig. 10) are more in agreement with a source in mantle enriched by slab-derived fluids than by fractional crystallization from lamprophyre, which is also enriched. Their negative Nb and Ti anomalies support this hypothesis. When transition elements are plotted against Ni on a log-scale diagram (not shown), some elements (e.g. Cr) display a linear relationship, suggesting that fractional crystallization has played some role during differentiation. Therefore, their maximum Ni (up to 124 ppm) and Cr (up to 473 ppm) contents are lower than that expected for primitive mantle magmas (Wilkinson and Le Maitre, 1987).

Generation of the continuous Paleoproterozoic igneous rock spectrum described from SerN, which ranges from tholeiite (IRGB) to high-K calc-alkaline rocks (IRGB and 2.15 Ga granites and TTGs), syenite, and shoshonite, is considered to be common during arc evolution where syenite represents the end-member. There is also a remarkable similarity between MASP rocks and minette and lamproite described in the literature (Rock et al., 1991; Mitchell and Bergman, 1991; Plá Cid et al., 2006).

Other studies have shown that TNT depletion and LILE enrichment in both Archaean (e.g. Superior Province, Canada; Wyman and Kerrich, 1989; Bourne and L'Heureux, 1991) and younger suites (e.g. Central Italy; Peccerillo et al., 1984, 1988), are common features. Also shown in Fig. 10 are average curves for rocks from subduction-related orogenic to post-orogenic environments such as Kirkland Lake syenite (3) and lamprophyre (1; Wyman and Kerrich, 1988); Italian potassic lavas (5; Thompson et al., 1982); the Clericy pluton, a typical Archaean ultrapotassic syenite from Canada (Bourne and L'Heureux, 1991). It is important to note that in the lamprophyre cumulates, i.e. the closest proxy of the composition of the liquid from which the syenite is believed to have evolved (Plá Cid et al., 2006), the general form of the extended trace element plots is similar to that of lamproite.

Fig. 13. Nb/Zr diagram proposed by Leat et al. (1986) to discriminate the potassic rocks, volcanic or plutonic, correlated or not to orogenic environments.

MASP rocks also show both highly enriched incompatible elements and highly depleted compatible element signatures (high Mg/Fe, low Ca). Mitchell and Bergman (1991) argue that these geochemical features are typical of lamproite, which originate in lithospheric upper mantle depleted by extraction of Ca- and Fe-rich basaltic melts and subsequently enriched in K and other LILE. At Monte Cimino, Italy, Perini et al. (2003) suggest that incorporation of K-feldspar megacrysts by mixing/mingling between mafic and felsic magmas resulted in a lowering of $^{87}Sr/^{86}Sr$ ratios and incompatible trace element contents of lamproite ultrapotassic magma. This could explain the low initial Sr ratios and similarities with lamproite shown by MASP rocks.

8.5. A source model for SerN potassic–ultrapotassic magmas

The Paleoproterozoic (2.2–2.0 Ga) was a time of extensive continental collision and growth. New terrains were being accreted to the Archaean nuclei at São Francisco Craton (Cordani et al., 2000). Based on the Nd-model ages (2.56–2.58 Ga), the precursor enrichment of the MASP mantle source may have taken place a long time before the Paleoproterozoic magmatic event. Based on whole rock Ar–Ar, K–Ar and Sm–Nd studies, the stabilization of the Itapicuru River Greenstone Belt (following the Transamazonian Orogeny) is considered to have occurred at 2.2–2.1 Ga (Silva, 1992). Contrasting Paleoproterozoic–Archaean U–Pb zircon ages for another metavolcano-sedimentary sequence, the Capim Group, which shows chemical characteristics similar to IRGB, are also available (2.1–2.2 and 2.5–2.8 Ga, Oliveira et al., 1998, 1999, 2002). These authors also present Nd T_{DM} ages for the IRGB of ~2.5 Ga, which indicates a rapid thickening of the Archaean lithosphere. Also, the Braúna kimberlite suite in southwestern SerN consists of 15 pipes and dikes having Rb–Sr phlogopite Neoproterozoic ages (682 ± 20 Ma), that intrude the southern area of Nordestina Batholith near the Maria Preta Mine and MASP (Pereira et al., 1996; Pisani et al., 2001; Pereira, 2001; Pereira and Fuck, 2005). These new data reinforce the idea that the origin of ultrapotassic rocks at SerN is related to a thick Archaean crust.

The location of ultrapotassic magmas at MASP, northwest of the proposed location of the SerN suture, suggests that the subducting slab was dipping to the northeast. Bergman (1987) and Mitchell and Bergman (1991) argue that the tectonic setting and composition of many lamproite bodies suggest that they include partial melts of fossil Benioff zones and most ultrapotassic rocks with negative Nb anomalies from well studied cra-

tons are though to be related to former subduction zones (e.g. Wyman and Kerrich, 1989; Larsen and Rex, 1992).

The presence of inherited zircon crystals, together with the depleted mantle Nd model ages (2.56–2.58 Ga) of MASP syenite and their Nd–Sr data suggest that LILE enrichment could be related to late Archaean subduction during assembly of the SerN at about 2.6–2.8 Ga (Rios, 2002; Rios et al., 2003). Therefore, actually, the presence of xenocrystic zircon suggests that crustal assimilation is the main reason for the Nd–Sr ratios. The presence of other Paleoproterozoic alkaline rocks in Bahia State that plot within the Nd and Sr isotope fields of MASP rocks (Conceição et al., 2002) also indicates that they all probably had the same formation mechanisms, but it does not indicate what the mechanism was. A similar proposal was made by Peterson et al. (2002) for rocks from Western Churchill Province (Canada).

These data suggest that the origin of K-rich magmatism in the SerN, which characterized the last 40 Ma of igneous activity (2.07–2.11 Ga; Rios et al., 2003, 2004), could be related to an older accretionary tectonic regime. Ultrapotassic rocks like these ones are also described in the Abitibi greenstone belt (Card, 1990; Laflèche et al., 1991). However the Abitibi belt is different in that it is juvenile Neoarchean and there was no pre-existing much older continental crust that got reworked in that area. Studies regarding Abitibi rocks suggest the presence of a primitive form of plate subduction at the Superior Province during the late Archaean. The same seems to be true at SerN, although its ultrapotassic rocks show Paleoproterozoic ages. The crystallization ages of MASP rocks are around 500 Ma younger than the hypothetical ~2.6 Ga slab, but felsic crust and metasomatized mantle, the products of this subduction, could have been stored in the lithosphere and melted during a much later accretionary event as occurred in West Greenland (Larsen and Rex, 1992).

In fact, it is not possible to rule out the possibility that Archean mantle metasomatism could have formed the source rocks for these alkaline magmas, while the fact that the alkaline magmas follow a period of Paleoproterozoic subduction would imply that later activity as the agent of metasomatism. Either way the 2.6–2.8 Ga Nd model ages, also presented by other syenite bodies from Bahia State, reinforce the idea of Archaean metasomatism.

9. Final remarks

Combined petrological, geochemical and geochronological studies on syenitic rocks from MASP confirm the co-existence of potassic and ultrapotassic suites in

the northeast part of São Francisco Craton. On the basis of our data we propose that the close spatial and temporal relationship between syenite and lamprophyre in Serrinha Nucleus is the result of a post-collisional arc setting and the intrusion of mantle-derived magmas into the orogen at this time.

MASP rocks show a subduction zone trace element signature and a ca. 2.6 Ga late Neoarchaean model age, in spite of being situated in Archaean crust with little evidence of rocks this young. Syenite magma at MASP was mainly formed by crystal fractionation from a parental lamprophyre magma (Plá Cid et al., 2006). Based on its lamproite affinities, the presence of K-feldspar xenocrysts and syenite xenolith material preserved in lamprophyres, as well as other textural evidence such as resorption zones and bodies of lamproite and kimberlite described in the region of SerN, we suggest that ultrapotassic lamprophyre at MASP represents a parental lamproite magma contaminated by interaction with syenite and other crustal granite components. This diluted the magma in compatible and incompatible elements.

Evidence of consanguinity between syenite and lamprophyre at MASP indicates that fractional crystallization played a very important role in the evolution of MASP. This association between syenite and potassic lamprophyre also has been noted by others as typical of early post-orogenic intrusions (Rock and Hunter, 1987; Eklund et al., 1998; Peterson et al., 2002), which can be associated with rare metal deposits and gold (Thompson and Fowler, 1986; Müller and Groves, 2000).

In summary, during the Paleoproterozoic (∼2.1 Ga), large volumes of syenite magma, with subordinate mafic and lamprophyre magma, intruded the São Francisco Craton. MASP is considered representative of this ultrapotassic suite and is closely comparable in age to others occurring over a wide area in diverse settings across the SFC. We propose that the similar ages of Bahia syenite potassic–ultrapotassic plutons reflect a large scale, craton-wide ultrapotassic magmatic event at ca. 2100 Ma. We speculate that this event reflects mantle that was metasomatized by fluids derived from earlier (Archaean?) descending slabs.

References

Alves da Silva, F.C., 1994. Étude Structural duo "Greenstone Belt" Paleoproterozoique du Rio Itapicuru (Bahia, Brésil). Thése Doct., Tese de Doutorado. Université d'Orleans, França, p. 307.

Alves da Silva, F.C., Chauvet, A., Faure, M., 1993. Early-Proterozoic (Tranzamazonian) Orogeny and syntectonic granite emplacement in the RIGB, Bahia, Brazil. Académie des Sciences (Paris) 316 (2), 1139–1146.

Atkinson, W.J., Hughes, F.E., Smith, C.B., 1984. A review of kimberlitic rocks of Western Australia. Kimberlites I: The Mantle and Crust-Mantle Relationships. In: Kornprobst, J. (Ed.), Kimberlites I: The Mantle and Crust-Mantle Relationships. Proc. 3rd Int. Kimb. Conf. Elsevier, Amsterdam, pp. 195–224.

Barbarin, B., 1991. Enclaves of the Mesozoic calc-alkaline granitoids of the Sierra Nevada Batholith, California. Enclaves and Granite Petrology. In: Didier, J., Barbarin, B. (Eds.), Dev. Petrol., vol. 3. Elsevier, Amsterdam, pp. 135–153.

Barbosa, J., Sabaté, P., 2004. Archean and Paleoproterozoic crust of the São Francisco Craton, Bahia, Brazil: geodynamic features. Precambrian Res. 133, 1–27.

Barrueto, H.R., 1997. Intrusões sub-vulcânicas alcalinas e lamprófiros nas mineralizações auríferas do GBRI, Bahia: petrografia, geoquímica e inclusões fluidas. Dissert. Mestrado. Pós-Graduação em Geociências, Unicamp, SP, p. 160.

Beccaluva, L., Di Girolamo, P., Serri, G., 1991. Petrogenesis and tectonic setting of the Roman Volcanic Province, Italy. Lithos 26, 191–221.

Bergman, S.C., 1987. Lamproites and other potassium-rich igneous rocks: a review of their occurrences, mineralogy and geochemistry. In: Fitton, J.G., Upton, B.G.J. (Eds.), Alkaline Igneous Rocks. In: Fitton, J.G., Upton, B.G.J. (Eds.), Geolf. Soc. Sp. Publ., vol. 30. pp. 103–226.

Blake, S., Koyaguchi, T., 1991. Insights on the magma mixing model from volcanic rocks. In: Diddier, J., Barbarin, B. (Eds.), Enclaves and Granite Petrology. In: Diddier, J., Barbarin, B. (Eds.), Developments in Petrology, vol. 13. Elsevier, Amsterdam, pp. 403–413.

Bourne, J.H., L'Heureux, M., 1991. The petrography and geochemistry of the Clericy Pluton: an ultrapotassic pyroxenite-syenite suite of late Archaean age from the Abitibi region, Quebec. Precambrian Res. 52 (1/2), 37–51.

Card, K.D., 1990. A review of the Superior Province of the Canadian Shield, a product of Archean accretion. Precambrian Res. 48, 99–156.

Conceição, H., 1990. Petrologie du massif syénitique d'Itiuba: contribution à l'etude minéralogique des roches alcalines dans l'Etat de Bahia (Brésil). Thése Doct. Université Paris-Sud, Centre d'Orsay, p. 395.

Conceição, H., Oliveira, O.M.C., Martin, H., Rosa, M.L.S., Conceição, R.V., Plá Cid, J., 1997. Petrologia do magmatismo alcalino potássico com afinidade lamprofírica e assinatura de subducção no sul do estado da Bahia: Maciço Sienítico de Anurí. Geochim. Brasil. 11 (2), 171–186.

Conceição, H., Rios, D.C., Rosa, M.L.S., 1995. Petrologia da Associação Sienito-Lamprófiro: Caso da Intrusão de Morro do Afonso (Greenstone Belt do Rio Itapicuru Bahia). Geoch. Brasil. 9 (1), 91–109.

Conceição, H., Rios, D.C., Rosa, M.L.S., Davis, D.W., Dickin, A.P., McReath, I., Marinho, M.M., Macambira, M.J.B., 2002. Zircon geochronology and petrology of alkaline-potassic syenites, southwestern Serrinha Nucleus, East São Francisco Craton. Brazil. Int. Geol. Rev. 44 (2), 117–136.

Conceição, H., Rosa, M.L.S., Macambira, M.J.B., Scheller, T., Marinho, M.M., Rios, D.C., 2003. 2.09 Ga Idade mínima da cristalização do Batólito Sienítico Itiúba: um problema para o posicionamento do clímax do metamorfismo granulítico (2.05–2.08 Ga) no Cinturão Móvel Salvador-Curaçá, Bahia? Rev. Bras. Geociências 33 (3), 391–394.

Conceição, R.V., Rosa, M.L.S., Nardi, L.V., Conceição, H., Lafon, J.M., Soliani, E., Oberli, F., Maier, M., Martin, H., 1999. Geochronology and isotopic signature of the Paleoproterozoic Santanápolis syenite (Bahia, Brazil). In: Proceedings of the Second South American Symposuim on Isotope Geology, Cordoba, Argentina, Actas, pp. 171–178.

Cordani, U.G., Milani, E.J., Thomaz Filho, A., Campos, D.A. (Eds.), 2000. Proceedings of the 31st International Geological Congress. Rio de Janeiro, RJ, p. 856.

Cordani, U.G., Sato, K., Marinho, M.M., 1985. The geologic evolution of the ancient granite-greenstone terrane of central southern Bahia, Brazil. Precambrian Res. 27, 187–213.

Corriveau, L., Gorton, M.P., 1993. Coexisting K-rich alkaline and shoshonitic magmatism of arc affinities in the Proterozoic: a reassessment of syenitic stocks in the southwestern Greenville Province. Contrib. Mineral. Petrol. 113, 262–279.

Cox, K.G., Bell, J.D., Pankhurst, R.J., 1979. The Interpretation of Igneous Rocks. George, Allen and Unwin, London, p. 450.

Davison, I., Teixeira, J.B.G., Silva, M.G., 1988. The Itapicuru Greenstone Belt, Bahia, Brazil: structure and stratigraphical outline. Precambrian Res. 42 (1–2), 1–17.

De Paolo, D.J., Schubert, G., 1991. The continental age distribution: methods of determining mantle separation ages from Sm–Nnd isotopic data and application to the southwestern United States. J. Geophys. Res. 96, 2071–2088.

Dorais, M.J., 1990. Compositional variations in pyroxenes and amphiboles of the Belknap Mountain complex, New Hampshire: evidence for origin of silica-saturated alkaline rocks. Am. Miner. 72, 1092–1105.

Doumbia, S., Pouclet, A., Kouamelan, A., Peucat, J.J., Vidal, M., Delor, C., 1998. Petrogenesis of juvenile-type Birimian (Paleoproterozoic) granitoids in Central Côte-d'Ivoire, West Africa: geochemistry and geochronology. Precambrian Res. 87, 33–63.

Eklund, O., Konopelko, D., Rutansen, H., Fröjdö, C., Shebanov, A.D., 1998. 1.8 Ga Svelojennaina post collisional shoshonitic magmatism in Fennoscandian Shield. Lithos 45, 87–108.

Evensen, N.M., Hamilton, P.J., Onions, R.K., 1978. Rare earth abundances in chondritic meteorites. Geochim. Cosmochim. Acta 42, 1199–1212.

Faure, G., 1986. Principles of Isotopic Geology. Wiley and Sons, New York, p. 589.

Fernandez, A.N., Barbarin, B., 1991. Relative rheology of coeval mafica and felsic magmas: nature of resulting interaction process. Shape and mineral fabrics of mafic microgranular enclaves. In: Diddier, J., Barbarin, B. (Eds.), Enclaves and Granite Petrology. In: Didier, J., Barbarin, B. (Eds.), Developments in Petrology, vol. 13. pp. 263–276.

Figueiredo, M.C.H., 1989. Geochemical evolution of eastern Bahia Brazil: a probably Early-Proterozoic subduction-related magmaticarc. J. South Am. Earth Sci. 2 (2), 131–145.

Foley, S.F., Peccerillo, A., 1992. Potassic and ultrapotassic magmas and their origin. Lithos 28, 181–185.

Foley, S.F., Venturelli, G., Green, D.H., Toscani, L., 1987. The ultrapotassic rocks: characteristics, classification and constrains for petrogenetic models. Earth Sci. Rev. 24, 81–134.

Gaudette, H.E., Lafon, J.M., Macambira, M.J.B., Moura, C.A.V., Scheller, T., 1998. Comparison of single filament Pb evaporation/ionization zircon ages with conventional U–Pb results: examples from the Precambrian of Brazil. J. South Am. Earth Sci. 11, 351–363.

Green, T.H., 1980. Island arc and continental building magmatism—a review of petrogenetic models based on experimental petrology and geochemistry. Tectonophysics 63, 367–385.

Irvine, T.N., Baragar, W.R.A., 1971. A guide to the chemical classification of the common volcanic rocks. Can. J. Earth Sci. 8, 523–548.

Jaffey, A.H., Flynn, K.F., Glendenin, L.E., Bentley, W.C., Essling, A.N., 1971. Precision measurement of half-lives and specific activities of ^{235}U and ^{238}U. Phys. Rev. 4, 1889–1906.

Jardim de Sá, E.F., 1982. Nota sobre o estilo estrutural e relações gnaisses vs. supracrustais no Greenstone Belt de Serrinha, Ba. Ciências da Terra 2, 8–13.

Köber, B., 1986. Whole-grain evaporation for $^{207}Pb/^{206}Pb$ age investigations on single zircons using a double filament thermal ion source. Contrib. Mineral. Petrol. 93, 482–490.

Köber, B., 1987. Single-zircon evaporation combined with Pb+ emitted bedding for $^{207}Pb/^{206}Pb$ age investigations using thermal ion mass spectrometry, and implications to zirconology. Contrib. Mineral. Petrol. 96, 63–71.

Laflèche, M.R., Dupuy, C., Dostal, J., 1991. Archaean orogenic ultrapotassic magmatism: an example from the Southern Abitibi greenstone belt. Precambrian Res. 52, 71–96.

Larsen, L.M., Rex, D.C., 1992. A review of the 2500 Ma span of alkaline-ultramafic potassic and carbonatitic magmatism in West Greenland. Lithos 28, 267–402.

Lavecchia, G., Stoppa, F., 1990. The Tyrrhenian zone: a case of lithosphere extension control of intracontinental magmatism. Earth Planet. Sci. Lett. 99, 336–350.

Lavecchia, G., Stoppa, F., 1996. The tectonic significance of Italian magmatism: an alternative view to the popular interpretation. Terra Nova 8, 435–446.

Leat, P.T., Jackson, S.E., Thorpe, R.S., Stillman, C.J., 1986. Geochemistry of bimodal basalt-subalkaline/peralkaline-rhyolite provinces within the southern British Caledonides. J. Geol. Soc. London 143, 259–276.

Lubala, R.T., Frick, C., Rogers, J.H., Walraven, F., 1994. Petrogenesis of syenites and granites of the Schiel Alkaline Complex Northern Transvaal. S. Afr. J. Geol. 102, 307–316.

Ludwig, K.R., 1999. Isoplot/Ex (version 2.00). A geochronological toolkit for Microsoft Excel. Berkeley Geochronology Center Special Publication Nr 1a, 46 pp.

Lynch, D.J., Musselman, T.E., Gutmann, J.T., Patchett, P.J., 1993. Isotopic evidence for the origin of Cenozoic volcanic rocks in the Pinacate volcanic field, Northwestern Mexico. Lithos 29, 295–302.

Mascarenhas, J.F., Pedreira, A.J.C.L., Gil, C.A.A., Neves, J.P., Oliveira, J.E., Silva Filho, M.A., Marinho, M.M., 1979. Geologia da região centro-oriental da Bahia. Projeto Bahia, Bahia II, Sul da Bahia. Relatório integrado. CPRM/DNPM, Brasília, DF, p. 128.

McNeil, A.M., Kerrich, R., 1986. Archean lamprophyre dykes and gold mineralization, Matheson, Ontario: the conjunction of LILE-enriched mafic magmas, deep crustal structures, and Au concentration. Can. J. Earth Sci. 23, 324–343.

Mitchell, R.H., Bergman, S.C., 1991. Petrology of Lamproites. Plenum Press, New York, p. 410.

Müller, D., Groves, D.I., 1993. Direct and indirect associations between potassic igneous rocks, shoshonites, and gold–copper deposits. Ore Geol. Rev. 8, 383–406.

Müller, D., Groves, D.I., 1995. Potassic Igneous Rocks and Associated Gold–copper Mineralization. Lecture Notes in Earth Sciences. Springer-Verlag, Berlin, p. 210.

Müller, D., Groves, D.I., 2000. Potassic Igneous Rocks and Associated Gold–Copper Mineralization. Springer, Berlin, 252 pp.

Müller, D., Rock, N.M.S., Groves, D.I., 1992. Geochemical discrimination between shoshonitic and potassic volcanic rocks from different tectonic settings: a pilot study. Mineral. Petrol. 46, 259–289.

Oliveira, E.P., Carvalho, M.J., Duarte, M.I.D., 2002. Extrusion of the Archaean Uauá Block during PalaeoproterozoicPalaeoproterozoic-Paleoproterozoic continent-continent collision northern segment of the Itabuna-Salvador-Curaçá Orogen Bahia. In: Proceedings of the XLI Congresso Brasileiro de Geologia, João Pessoa, Anais, p. 324.

Oliveira, E.P., Lafon, J.-M., Souza, Z.S., 1998. A Paleoproterozoic age for the Rio Capim volcano–plutonic sequence, Bahia, Brazil: whole-rock Pb–Pb Pb–evaporation and U–Pb constraints. In: Anais XI Congresso Brasileiro de Geologia. SBG, Belo Horizonte, MG, p. 14.

Oliveira, E.P., Lafon, J.-M., Souza, Z.S., 1999. Archaean–Paleoproterozoic transition in the Uauá Block, NE Sãao Francisco Craton, Brazil: U–Pb, Pb–Pb and Nd isotope constraints. In: Proceedings of First International Symposium on Tectonics of the Brazilian Geological Society, Lençois, BA, pp. 49–51 (abstract-volume).

Paim, M.M., Pla Cid, J., Rosa, M.L.S., Conceição, H., Nardi, L.V.S., 2002. Mineralogy of lamprophyres and mafic enclaves associated with the PalaeoproterozoicPalaeoproterozoicPaleoproterozoic Cara Suja Syenite, Northeast Brazil. Int. Geol. Rev. 44 (11), 1017–1036.

Pearce, J.A., 1983. Role of the subcontinental lithosphere in magma geênesis at active continental margins. In: Hawkesworth, C., Norry, W.J. (Eds.), Continental Basalts and Mantle Xenoliths. Shiva Publications, London, pp. 230–250.

Pearce, J.A., Cann, J.R., 1973. Tectonic setting of basic volcanic rocks determined using trace element analyses. Earth Planet. Sci. Lett. 19, 290–300.

Pearce, J.A., Harris, N.B.W., Tindle, A.G., 1984. Trace element discrimination diagrams for the tectonic interpretation of granitic rocks. J. Petrol. 25, 956–983.

Pearce, J.A., Norry, M.J., 1979. Petrogenetic implications of Ti, Zr, Y and Nb variations in volcanic rocks. Contrib. Mineral. Petrol. 69, 33–47.

Peaucat, J.J., Capdevila, R., Drareni, A., Mahdjoub, Y., Kahoui, M., 2005. The Eglab massif in the West Africa Craton (Algeria), an original segment of the Eburnean orogenic belt: petrology, geochemistry, geochronology. Precambrian Res. 136, 309–352.

Peccerillo, A., 1992. Potassic and ultrapotassic magmatism: compositional characteristics, genesis and geologic significance. Episodes 15, 243–251.

Peccerillo, A., Poli, G., Serri, G., 1988. Petrogenesis of orenditic and kamafugitic rocks from Central Italy. Can. Mineral. 26, 45–65.

Peccerillo, A., Poli, G., Tolomeo, L., 1984. Genesis, evolution and tectonics significance of K-rich volcanics from the Alban Hills (Roman Comagmatic Region) as inferred from trace element geochemistry. Contrib. Mineral. Petrol. 86, 230–240.

Pereira, R.S., 2001. Técnicas exploratórias na prospecção de kimberlitos—estudo de caso. Rev. Bras. Geociências 31 (4), 405–416.

Pereira, R.S., Fuck, R.A., 2005. Kimberlitos e rochas relacionadas no Cráton do São Francisco. In: Proceedings of the III Symposium on the São Francisco Cráton, SBG, pp. 114–117.

Pereira, R.S., Zang, M., Bizzi, L, 1996. Target selection in the Bahia Project Area using regional scale geophysics, remote sensing and geochemistry. Geophysical Services Division, Sopemi, Brasília, unpublished.

Perini, G., Tepley III, F.J., Davidson, J.P., Conticelli, S., 2003. The origin of K-feldspar megacrysts hosted in alkaline potassic rocks from Central Italy: a track for low-pressure processes in mafic magmas. Lithos 66, 223–240.

Peterson, T.D., Van Breemen, O., Sandeman, H., Cousens, B., 2002. Proterozoic (1.85–1.75 Ga) igneous suites of the Western Churchill Province: granitoid and ultrapotassic magmatism in a reworked Archaean hinterland. Precambrian Res. 119, 73–100.

Peucat, J.-J., Capdevila, R., Drareni, A., Mahdjoub, Y., Kahoui, M., 2005. The Eglab massif in the West African Craton (Algeria), an original segment of the Eburnean orogenic belt: petrology, geochemistry and geochronology. Precambrian Res. 136, 309–352.

Pisani, J.R.T., Tainton, K.M., Allan, A.F., Silva, S.B., Miranda, J.V., 2001. Geology and exploration of the Braúna Diamondiferous Kimberlites, Serrinha Block, Bahia, Brazil. Rev. Bras. Geociências 31 (4), 663–664.

Plá Cid, J., Rios, D.C., Conceição, H., 2006. Petrogenesis of mica–amphibole-bearing lamprophyres associated with the Paleoproterozoic Morro do Afonso syenite intrusion, eastern Brazil. J. South Am. Earth Sci. 22, 98–115.

Rios, D.C., 1998. Petrologia do Magmatismo Potássico-Ultrapotássico e Lamprofírico de Morro do Afonso-Bahia. In: Conceição, H., Cruz, M.J.M. (Eds.), Sienitos Alcalinos Potássicos e Ultrapotássicos Paleoproterozóicos do Estado da Bahia, vol. 4. Publicação Especial da Sociedade Brasileira de Geologia, Núcleo Bahia-Sergipe, Salvador, BA, pp. 167–204.

Rios, D.C., 1997. Petrologia do magmatismo potássico-ultrapotássico e lamprofírico de Morro do Afonso-Bahia. Unpub. Dissertação de Mestrado. Universidade Federal da Bahia, 237 p.

Rios, D.C., 2002. Granitogênese no Núcleo Serrinha, Bahia, Brasil: Geocronologia e Litogeoquímica. Unpub. PhD Thesis. Federal University of Bahia, 239 p.

Rios, D.C., Conceição, H., Davis, D.W., Rosa, M.L.S., Macambira, M.J.B., Peixoto, A.A., Marinho, M.M., 2006. Morro do Lopes Granites: Palaeoproterozoic alkaline magmas and their significance for Serrinha Nucleus evolution, Northeastern Bahia, Brazil. In: South American Symposium on Isotope Geology, 2006, Punta del Este. Short Papers of the V South American Symposium on Isotope Geology, Punta del Este, vol. 1, Universidad de la República, pp. 162–164.

Rios, D.C., Conceição, H., Davis, D.W., Rosa, M.L.S., Macambira, M.J.B., Dickin, A.P., 2003. A new proposal for the subdivision of granitic rocks at Serrinha Nucleus, Bahia, Brazil, based on U–Pb and Pb–Pb geochronological and litogeochemical data. Proceedings of the IV South American Symposium on Isotope Geology, Brazil, Short Papers, vol. 1, pp. 264–267.

Rios, D.C., Conceição, H., Davis, D.W., Rosa, M.L.S., Marinho, M.M., 2005. Expansão do magmatismo pós-orogênico no Núcleo Serrinha (NE Bahia) Cráton do São Francisco: Idade U–Pb do maciço granítico Pedra Vermelha. Rev. Bras. Geociências 35 (3), 423–426.

Rios, D.C., Davis, D.W., Conceição, H., Macambira, M.J.B., Peixoto, A.A., Cruz Filho, B.E., Oliveira, L.L., 2000. Ages of granites

of the Serrinha Nucleus, Bahia (Brazil): an overview. Rev. Bras. Geociências 30, 74–77.

Rios, D.C., Davis, D.W., Conceição, H., Rosa, M.L., Dickin, A.P., 2004. Archaean granites at Serrinha Nucleus, Bahia, Brazil. Geochim. Cosmochim. Acta 68 (11), A685.

Rios, D.C., Davis, D.W., Conceição, H., Rosa, M.L., Marinho, M.M., 2002. The oldest zircons from South Ameérica Continent. Geochim. Cosmochim. Acta 66 (A345), 640.

Rios, D.C., Conceição, H., Macambira, M.J.B., Burgos, C.M.G., Peixoto, A.A., Cruz Filho, B.E., Oliveira, L.L., Lisboa, M.P., 1998. Granitogênese da parte meridional-oriental do Núcleo Serrinha: idade, petrografia e geoquímica. In: Conceição, H., Cruz, M.J.M., Sá, H.J.S., Sabaté, P. (Eds.), Contribuição ao estudo dos granitos e rochas correlatas., vol. 5. Pub. Esp. SBG, Núcleo Bahia, Sergipe, pp. 91–113.

Rock, N.M.S., 1987. Nature and origin of calc-alcaline lamprophyres: an review. In: Fitton, J.G., Upton, B.G.J. (Eds.), Alkaline Igneous Rocks, vol. 30. Geological Society Special Publication, pp. 191–226.

Rock, N.M.S., Bowes, D.R., Wright, A.E., 1991. Lamprophyres. Blackie-Van Nostrand Reinhold, New York, p. 285.

Rock, N.M.S., Groves, D.I., 1988. Can lamprophyres resolve the genetic controversy over mesothermal gold deposits? Geology 16, 538–541.

Rock, N.M.S., Hunter, R.H., 1987. Late Caledonian dyke-swarms of northern Britain: spatial and temporal intimacy between lamprophyric and granitic magmatism around the Ross of Mull pluton. Inner Hebrides. Geol. Rundsch. 76, 805–826.

Rogers, G., Saunders, A.D., Terrel, D.J., Verma, S.P., Marriner, G.F., 1985. Geochemistry of Holocene volcanic rocks associated with ridge subduction in Baja Califórnia, México. Nature 315, 389–392.

Rosa, M.L.S., Conceição, H., Macambira, M.J.B., Galarza, M.A., Cunha, M.P., Menezes, R.C.L., Marinho, M.M., Cruz Filho, B.E., Rios, D.C., 2006. Neoproterozoic anorogenic magmatism in the Southern Bahia Alkaline Province of NE Brazil: U-Pb and Pb-Pb ages of the blue sodalite syenites. Lithos, doi:10.1016/j.lithos.2006.12.011.

Rosa, M.L.S., Conceição, H., Macambira, M.J.B., Scheller, T., Martin, H., Leal, L.R.B., 2001. Idade (Pb–Pb) e assinatura isotópica (Rb–Sr, Sm–Nd) do magmatismo sienítico pPaleoproterozóico no sul do Cinturão Móvel Salvador-Curaçá: Maciço sienítico de São Félix (Bahia). Rev. Bras. Geociências 31 (3), 397–400.

Rosa, M.L.S., Conceição, H., Oberli, F., Meier, M., Martin, H., Macambira, M.J.B., Santos, E.B.S., Paim, M.M., Leahy, G.A.S., Leal, L.R.B., 2000. Geochronology (U–Pb/Pb–Pb) and isotopic signature (Rb–Sr/Sm–Nd) of the Ppaleoproterozoic Guanambi Batholith, southwest Bahia State (NE, Brazil). Rev. Bras. Geociências 30 (1), 62–65.

Rosa, M.L.S., Conceição, H., Paim, M.M., Santos, E.B., Alves da Silva, F.C., Leahy, G.A.S., Leal, L.R.B., 1996. Magmatismo potássico-ultrapotássico pós a tardi-orogênico (associado à subducção) no oeste da Bahia: Batólito Monzo-Sienítico de Guanambi-Urandi e os sienitos de Correntina. Geoch. Brasil. 101 (1), 27–42.

Sato, K., Tassinari, C.C.G., Kawashita, K., Petronilho, 1995. O método geocronológico Sm–Nd no IG-USP e suas aplicações. An. Acad. Bras. Cienc. 67 (3), 313–336.

Schwarzar, R.R., Rogers, J.J., 1974. A world-wide comparison of olivine basalt and their differentiation trends. Earth Planet. Sci. Lett. 23, 286–296.

Serri, G., Innocenti, F., Manetti, P., 1993. Geochemical and petrological evidences of the subduction of delaminated Adriatic continental lithosphere in the genesis of the Neogene-Quaternary magmatism of central Italy. Tectonophysics 223, 117–147.

Silva, A.B., Liberal, G.S., Grossi Sad, J.M., Issa Filho, A., Rodrigues, C.S., Riffel, D.F., 1988. Geologia e Petrologia do Complexo Angico dos Dias (Bahia, Brasil), uma associação carbonática Precambrianapré-cambriana. Geochim. Brasil. 2 (1), 81–108.

Silva, M.G., 1992. O Greenstone Belt do Rio Itapicuru: uma bacia do tipo back-arc fóssil. Rev. Bras. Geociências 22, 157–166.

Silva, M.G., Coelho, C.E.S., Teixeira, J.B.G., Alves da Silva, F.C., Silva, R.A., Souza, J.A.B., 2001. The Rio Itapicuru greenstone belt, Bahia, Brazil: geologic evolution and review of gold mineralization. Miner. Deposita 36, 345–357.

Souto, P.G., 1972. Geologia e petrografia da área de Potiraguá, Bahia. Tese de Doutorado. Universidade de São Paulo, São Paulo, Brasil, p. 65.

Stacey, J.S., Kramers, J.D., 1975. Approximation of terrestrial lead isotope evolution by a two-stage model. Earth Planet. Sci. Lett. 26, 207–221.

Stern, R.A., 1997. The GSC Sensitive High Resolution Ion Microprobe (SHRIMP): analytical techniques of zircon U–Th–Pb age determinations and performance evaluation. In: Current Research 1997-F. Geological Survey of Canada: Radiogenic Age and Isotopic Studies Report 10, pp. 1–31.

Streckeisen, A., 1976. To each plutonic rocks its proper name. Earth Science Rev. 12, 1–33.

Sun, S.S., 1980. Lead isotopic study of young volcanics from midocean ridges, ocean islands and island arcs. Philos. Trans. R. Soc. Lond. A297, 409–445.

Sutcliffe, R.H., Smith, A.R., Doherty, W., Barnett, R.L., 1990. Mantle derivation of Archean—bearing granitoid and associated mafic rocks: evidence from the southern Superior Province. Contrib. Mineral. Petrol. 105, 255–274.

Tchameni, R., Mezger, K., Nsifa, N.E., Pouclet, A., 2001. Crustal origin of Early Proterozoic syenites in the Congo Craton (Ntem Complex), South Cameroon. Lithos 57, 23–42.

Thompson, R.N., 1982. Magmatism of the British Tertiary Volcanic Province. Scott. J. Geol. 18, 49–107.

Thompson, R.N., Dickin, A.P., Gibson, I.L., Morrison, M.A., 1982. Elemental fingerprints of isotopic contamination of Hebridean Paleocene mantle-derived magmas by Archean sial. Contrib. Mineral. Petrol. 79, 159–168.

Thompson, R.N., Fowler, M.B., 1986. Subduction-related shoshonitic and ultrapotassic magmatism: a study of siluro-ordovician syenites from Scottish caledonites. Contrib. Mineral. Petrol. 14, 507–522.

Vasconcelos, P., Becker, T., 1992. A idade da mineralização aurífera no depósito da Fazenda Brasileiro, Bahia, Brasil. Workshop em Metalogênese: Pesquisas atuais e novas tendencies. UNICAMP, Bol. Res., p. 29.

Watson, E.B., Harrison, T.M., 1983. Zircon saturation revisited: temperature and composition effects in a variety of crustal magma types. Earth Planet. Sci. Lett. 64 (2), 295–304.

Wilkinson, J.F.G., Le Maitre, R.W., 1987. Upper mantle amphiboles and micas and TiO_2, K_2O, and P_2O_5 abundances and $100\,Mg/(Mg + Fe_2 +)$ ratios of common basalts and andesites: implications for modal mantle metasomatism and undepleted mantle compositions. J. Petrol. 28, 37–73.

Wilson, M., 1989. Igneous Petrogenesis. Chapman & Hall, London, 466 pp.

Wyman, D.A., Kerrich, R., 1988. Alkaline magmatism, major structures, and gold deposits: implication for greenstone belt gold metallogeny. Econ. Geol. 83, 454–461.

Wyman, D.A., Kerrich, R., 1989. Archean lamprophyre dikes of the Superior Province, Canada: distribution, petrology, and geochemical characteristics. J. Geophys. Res. 94 (B4), 4667–4696.

Wyman, D.A., Kerrich, R., 1993. Archean shoshonitic lamprophyres of the Abitibi Subprovince, Canada: petrogenesis, age and tectonic setting. J. Petrol. 34 (6), 1067–1109.

Zhao, J.-X., Shiraishi, K., Ellis, D.J., Sheraton, J.W., 1995. Geochemical and isotopic studies of syenites from the Yamoto Mountains East Antartica: implication for the origin of syenitic magmas. Geochim. Cosmochim. Acta 59, 1363–1385.